Chebyshev collocation spectral lattice Boltzmann method for simulation of low-speed flows

Kazem Hejranfar* and Mahya Hajihassanpour
Department of Aerospace Engineering, Sharif University of Technology, Tehran, Iran
(Received 11 December 2013; revised manuscript received 8 June 2014; published 7 January 2015)

In this study, the Chebyshev collocation spectral lattice Boltzmann method (CCSLBM) is developed and assessed for the computation of low-speed flows. Both steady and unsteady flows are considered here. The discrete Boltzmann equation with the Bhatnagar-Gross-Krook approximation based on the pressure distribution function is considered and the space discretization is performed by the Chebyshev collocation spectral method to achieve a highly accurate flow solver. To provide accurate unsteady solutions, the time integration of the temporal term in the lattice Boltzmann equation is made by the fourth-order Runge-Kutta scheme. To achieve numerical stability and accuracy, physical boundary conditions based on the spectral solution of the governing equations implemented on the boundaries are used. An iterative procedure is applied to provide consistent initial conditions for the distribution function and the pressure field for the simulation of unsteady flows. The main advantage of using the CCSLBM over other high-order accurate lattice Boltzmann method (LBM)-based flow solvers is the decay of the error at exponential rather than at polynomial rates. Note also that the CCSLBM applied does not need any numerical dissipation or filtering for the solution to be stable, leading to highly accurate solutions. Three two-dimensional (2D) test cases are simulated herein that are a regularized cavity, the Taylor vortex problem, and doubly periodic shear layers. The results obtained for these test cases are thoroughly compared with the analytical and available numerical results and show excellent agreement. The computational efficiency of the proposed solution methodology based on the CCSLBM is also examined by comparison with those of the standard streaming-collision (classical) LBM and two finite-difference LBM solvers. The study indicates that the CCSLBM provides more accurate and efficient solutions than these LBM solvers in terms of CPU and memory usage and an exponential convergence is achieved rather than polynomial rates. The solution methodology proposed, the CCSLBM, is also extended to three dimensions and a 3D regularized cavity is simulated; the corresponding results are presented and validated. Indications are that the CCSLBM developed and applied herein is robust, efficient, and accurate for computing 2D and 3D low-speed flows. Note also that high-accuracy solutions obtained by applying the CCSLBM can be used as benchmark solutions for the assessment of other LBM-based flow solvers.

DOI: 10.1103/PhysRevE.91.013301 PACS number(s): 99.10.−x

I. INTRODUCTION

Over the past two decades, there has been rapid progress in developing and employing the lattice Boltzmann method (LBM) as an alternative computational fluid dynamics approach for simulating complex flows (see, for example, Refs. [1–6]). An alternative to the lattice-gas automata for studying hydrodynamic properties was introduced in Ref. [1] in which the lattice gas is modeled by a Boltzmann equation. In [2] it was shown that the lattice Boltzmann (LB) equation can provide a convenient alternative to the direct simulation of cellular automata microdynamics. This was one of the early efforts in applying LBM as an alternative solver for the conventional computational fluid dynamics (CFD) methods. An efficient strategy was proposed in Ref. [3] for the construction of appropriate collision operators, to be implemented in a simplified version of the LB equation to make the LBM competitive in the CFD area. More details on the basic elements of the LB equation can be found in Refs. [4,5]. The application of the LBM to simulate rarefied gas dynamics was made in Ref. [6].

The LBM has several advantages over other conventional CFD methods, especially in dealing with complex boundaries, incorporating microscopic interactions, and efficient parallelizing of its solution algorithm. The conventional LBM may not be suitable for problems with large pressure gradients because of the compressibility error [7]. Efforts to reduce the compressibility error in the incompressible form of the LBM are categorized in two different approaches: density-based methods [8–10] and pressure-based methods [11–14]. Density-based methods are appropriate for multicomponent or multiphase flows while pressure-based methods strictly solve the pressure variable and recover the incompressible Navier-Stokes equations.

Despite the increasing popularity of the LBM in simulating complex fluid systems, this approach has some limitations too. The standard LBM with the Bhatnagar-Gross-Krook (BGK) approximation is restricted to the use of uniform Cartesian grids with equal spacing that limit its applications to solve practical engineering problems. Inherent instability for simulating high-Reynolds-number flows is another drawback of this methodology [15]. Using a multi-relaxation-time version [16,17] and implementing the cascaded LBM [18,19] on nonuniform meshes are efforts that have been made in the literature to overcome these shortcomings.

Studies for improving the computational accuracy and efficiency of the LBM can be classified into two different categories [20]: namely, interpolation types and differential types. In the interpolation type, usually a coarse grid is initially used for the simulation of the entire domain and then a grid refinement procedure is applied to locally refine the grid in

*khejran@sharif.edu

the critical regions requiring a high grid resolution [20,21]. In the differential types, the LBM is considered as a particular discretization of the discrete Boltzmann equation (DBE) using the Taylor-series expansion in time and space [5]. Recently, several attempts have been made to use different computational fluid dynamics methods for solving the DBE. Spectral-element discontinuous Galerkin methods [22–24], finite-element methods [25–27], finite-volume methods [28–33], traditional finite-difference methods [34–43], and more recently the high-order compact finite-difference method [44] have been applied to improve the capability of the LBM in modeling different fluid flow problems accurately and efficiently.

For precisely predicting complex flows, high-order accurate numerical methods are to be used that reduce the grid and CPU time requirements compared to the traditional low-order numerical methods. Among different high-order accurate numerical methods, the spectral methods are known as suitable schemes that can resolve everything up to the smallest dynamical scales in the flow structures. Thus, they are more appropriate for performing direct numerical simulations (DNSs) of turbulent flows and computations of other critical applications [45–47]. On the other hand, the LBM formulation is much easier to use for modeling fluid flows compared to the solution of Navier-Stokes equations. Thus, applying the spectral methods for the solution of the LB equation provides a highly accurate and reliable DNS LBM flow solver that can be considered as an alternative to the DNS Navier-Stokes flow solvers. Note that high-accuracy solutions obtained by applying the spectral methods to the LBM formulation can be considered as benchmark solutions for the assessment of other LBM-based flow solvers developed in the literature.

The main objective of this paper is to develop and apply a Chebyshev collocation spectral lattice Boltzmann method (CCSLBM) for the simulation of low-speed flows. The decay of the error at exponential rather than polynomial rates is the main benefit of applying the Chebyshev collocation spectral LBM over other high-order LBM-based flow solvers. Another advantage of the proposed CCSLBM is that it does not require any numerical dissipation or filtering for the solution to be stable, which leads to highly accurate solutions. In general, spectral methods are quite sensitive to the implementation of boundary conditions and therefore special consideration should be paid to obtain accurate and stable solutions when applying such methods. In this study, instead of any *ad hoc* boundary condition, physical boundary conditions are implemented based on the solution of the governing equations applied at each boundary to obtain accurate and stable solutions. Herein, the spatial derivatives in the LB equation are discretized by using the Chebyshev collocation spectral method and the temporal term is discretized by the fourth-order Runge-Kutta scheme to provide an accurate and efficient low-speed flow solver. An iterative procedure based on the solution of the LB equation by applying the CCSLBM is implemented to provide consistent initial conditions for the distribution function and the pressure field for simulating unsteady flows. The accuracy and robustness of the proposed methodology, that is, the CCSLBM, are shown by simulating different two-dimensional (2D) or 3D low-speed flow problems at different conditions and the results obtained are thoroughly compared with the analytical and available numerical results. The accuracy and performance of the solution obtained by applying the CCSLBM are also examined by comparison with those of the standard streaming-collision (classical) LBM and two finite-difference LBM solvers, namely, the fourth-order compact finite-difference LBM (CFDLBM) [44] and the developed second-order central finite-difference LBM (FDLBM).

The paper is organized as follows. In Sec. II the LB equation for 2D low-speed flows based on the pressure distribution function is presented. In Sec. III the Chebyshev collocation spectral method and the Runge-Kutta time-stepping scheme are given. Section IV includes the initialization procedure to provide consistent initial conditions for simulating unsteady flows. The implementation of boundary conditions is presented in Sec. V. Section VI is devoted to presenting the results obtained by applying the CCSLBM for different 2D test cases. In Sec. VII the solution methodology is extended to three dimensions and the results of the simulation of a regularized cubic cavity are presented in Sec. VIII. Finally, a summary and conclusions are given in Sec. IX.

II. GOVERNING EQUATIONS

The Boltzmann equation governed the particle distribution function $f(t,e,x)$ is utilized with the single relaxation-time and the BGK approximation [48]

$$\frac{\partial f}{\partial t} + \boldsymbol{e}\cdot\nabla f = -\frac{1}{\tau}(f - f^{eq}), \tag{1}$$

where $\boldsymbol{e}$ is the particle velocity, τ is the dimensionless collision relaxation time, and f^{eq} is the equilibrium distribution function. With discretizing the velocity space $\boldsymbol{e}$, the lattice Boltzmann (LB) equation for the particle distribution function f_k in the direction of microscopic velocity $\boldsymbol{e}_k$ may be written as

$$\frac{\partial f_k}{\partial t} + \boldsymbol{e}_k\cdot\nabla f_k = -\frac{1}{\tau}\left(f_k - f_k^{eq}\right), \quad k = 0,1,\ldots,8, \tag{2}$$

where the subscript k denotes the direction of the particle speed. In the D2Q9 discrete Boltzmann model, the microscopic velocities (see Fig. 1) are given as

$$\mathbf{e}_k = \begin{bmatrix} e_{kx} \\ e_{ky} \end{bmatrix} = \begin{bmatrix} e_{0x} & e_{1x} & e_{2x} & e_{3x} & e_{4x} & e_{5x} & e_{6x} & e_{7x} & e_{8x} \\ e_{0y} & e_{1y} & e_{2y} & e_{3y} & e_{4y} & e_{5y} & e_{6y} & e_{7y} & e_{8y} \end{bmatrix} = \begin{bmatrix} 0 & 1 & 0 & -1 & 0 & 1 & -1 & -1 & 1 \\ 0 & 0 & 1 & 0 & -1 & 1 & 1 & -1 & -1 \end{bmatrix}. \tag{3}$$

The equilibrium distribution function f^{eq} is selected to satisfy the incompressible Navier-Stokes equations through a Chapman-Enskog expansion procedure. For low-speed flows, the density ρ_0 is approximately constant and the pressure p can

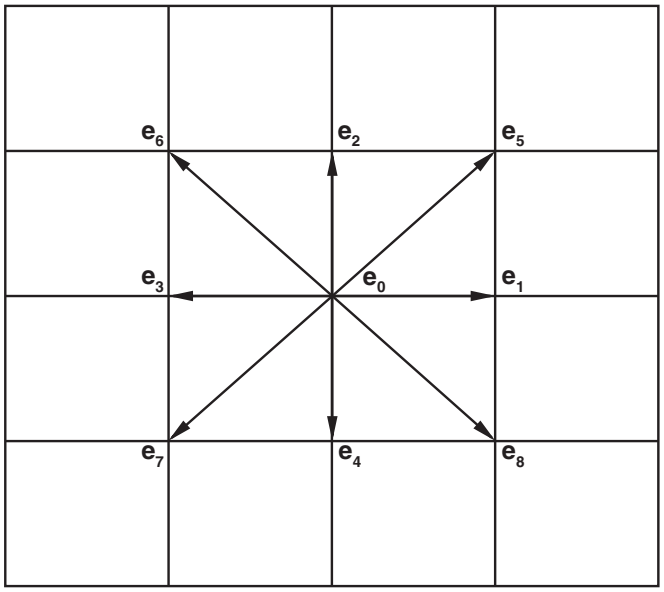

FIG. 1. The D2Q9 lattice and the microscopic velocities.

be used as an independent variable. The incompressible form of the LB equation used in this study is based on the model applied by He and Luo [12]. They suggested a local pressure distribution function by redefining the density distribution function in the LB equation, utilizing the fact that the error terms on the order of M^2 (M is the Mach number) are explicitly removed from the equilibrium distribution function. Thus, the incompressible form of the LB equation is solved to obtain the pressure in the computational domain and the fluid density is not calculated in the simulations. In this formulation, the equilibrium distribution function is defined as [12]

$$f_k^{eq} = \alpha_k \{ p + p_0 [3(\boldsymbol{e}_k \cdot \boldsymbol{u}) + \tfrac{9}{2}(\boldsymbol{e}_k \cdot \boldsymbol{u})^2 - \tfrac{3}{2}(\boldsymbol{u} \cdot \boldsymbol{u})] \}, \quad (4)$$

with $\alpha_0 = \frac{4}{9}$, $\alpha_1 = \alpha_2 = \alpha_3 = \alpha_4 = \frac{1}{9}$, and $\alpha_5 = \alpha_6 = \alpha_7 = \alpha_8 = \frac{1}{36}$ for the D2Q9 model, and $\boldsymbol{u} = (u, v)$ is the velocity vector.

The macroscopic pressure p and the macroscopic velocity vector $\boldsymbol{u}$ are obtained using the relations

$$p = \sum_{k=0}^{8} f_k, \quad p_0 \boldsymbol{u} = \sum_{k=0}^{8} \boldsymbol{e}_k f_k, \quad (5)$$

where $p_0 = c_s^2 \rho_0$ and ρ_0 is the constant density of the fluid. The incompressible Navier-Stokes equations can be derived from the incompressible form of the LB model through the Chapman-Enskog expansion procedure [12]:

$$\frac{1}{c_s^2} \frac{\partial P}{\partial t} + \nabla \cdot \boldsymbol{u} = 0, \quad (6)$$

$$\frac{\partial \boldsymbol{u}}{\partial t} + \boldsymbol{u} \cdot \nabla \boldsymbol{u} = -\nabla P + \upsilon \nabla^2 \boldsymbol{u}, \quad (7)$$

where $P = \frac{p}{\rho_0}$ is the normalized pressure and υ is the kinematic viscosity of the fluid. The relaxation time τ in this model is defined by [34]

$$\tau = \frac{\upsilon}{c_s^2}, \quad (8)$$

where $c_s = 1/\sqrt{3}$ is the speed of sound of the LB model.

Herein, it is the goal to simulate both steady and unsteady low-speed flows using the Chebyshev collocation spectral LBM. For steady flow computations, the term $\frac{\partial P}{\partial t}$ in Eq. (6) approaches zero by converging the solution, which leads the continuity equation to be exactly satisfied. For unsteady flow simulations, a further condition has to be satisfied [12], which is briefly discussed here. For this aim, the nondimensional form of incompressible Navier-Stokes equations (6) and (7) is given by

$$\begin{aligned} &\frac{1}{T} \frac{\partial P^*}{\partial t^*} + \frac{c_s}{L} \nabla^* \cdot \boldsymbol{u}^* = 0, \\ &\frac{1}{T} \frac{\partial \boldsymbol{u}^*}{\partial t^*} + \frac{c_s}{L} \boldsymbol{u}^* \cdot \nabla \boldsymbol{u}^* = -\frac{c_s}{L} \nabla^* P^* + \frac{\upsilon}{L^2} \nabla^{*2} \boldsymbol{u}^*, \end{aligned} \quad (9)$$

where the following scaling parameters are used:

$$l^* = \frac{l}{L}, \quad t^* = \frac{t}{T}, \quad u^* = \frac{u}{c_s}, \quad v^* = \frac{v}{c_s}, \quad P^* = \frac{P}{c_s^2} \quad (10)$$

and T and L are the characteristic time and length, respectively. The dimensionless form of the continuity equation shows that the term $\frac{\partial P^*}{\partial t^*}$ is negligible by considering the condition $T \gg L/c_s$, which means that the macroscopic characteristic time T should be chosen greater than the time taken by a sound signal to travel the length scale. This condition is satisfied in the discrete Boltzmann equation by selecting very slow temporal variations for the driving pressure in the simulation of unsteady flows [12]. This procedure has been used in Ref. [44] and led to accurate and reliable unsteady computations.

III. DISCRETIZATION PROCEDURE

In this study, the Chebyshev collocation spectral method is applied to solve the LB equation. To examine the resolution characteristics of such a highly accurate numerical method, the spectral function (or the modified wave number) associated with this scheme can be used (see Fig. 2). The modified wave number for the first derivative approximation of the spectral method is compared with two other numerical methods, namely, the fourth-order compact and second-order central finite-difference schemes, as plotted in Fig. 2. Note that for the exact differentiation, the modified wave number must be $\bar{\beta}(\beta) = \beta$. It is shown that the spectral method provides the exact solution, whereas two other finite-difference schemes deviate from the exact solution especially for high wave numbers.

Herein, the spatial derivatives in the LB equation are discretized by a Chebyshev collocation spectral method to obtain high-accuracy solutions. The series expansion for a sample function $u(\xi, t)$ may be approximated as [49–54]

$$u(\xi, t) = \sum_{n=0}^{N} \hat{u}_n(t) \phi_n(\xi), \quad (11)$$

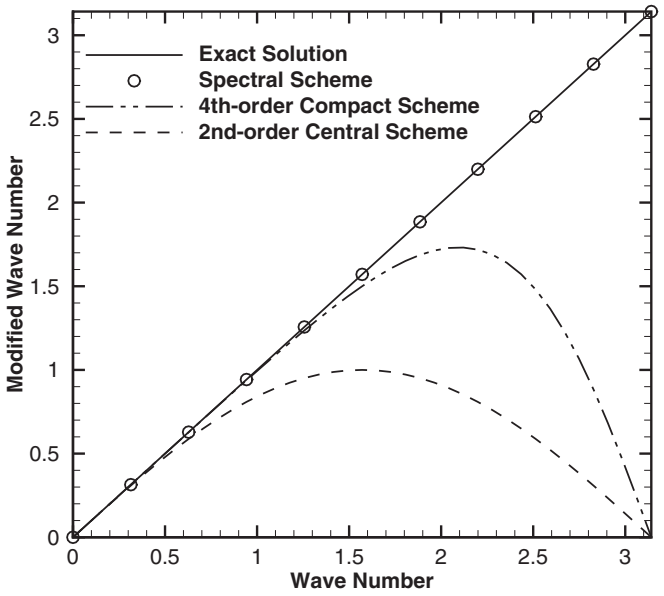

FIG. 2. Comparison of the modified wave number of the spectral scheme with the fourth-order compact and second-order central finite-difference schemes.

where $\phi_n(\xi)$ are the trial or basis functions, $\hat{u}_n(t)$ are the time-dependent expansion spectral coefficients, and N is the polynomial degree. For the Chebyshev collocation spectral method, the basis functions are the Chebyshev polynomials. In the most common Chebyshev collocation spectral method, the interpolation points in the interval $\xi = [-1,1]$ are the Chebyshev-Gauss-Lobatto collocation points $\xi_j = \cos(j\pi/N)$ for $j = 0,\ldots,N$, which are the extreme of the jth-order Chebyshev polynomials $T_j(\xi) = \cos[j\cos^{-1}(\xi)]$. The Chebyshev collocation spectral method is characterized by the fact that the numerical solution is forced to satisfy the equations exactly at the collocation points.

The expansion coefficients $\hat{u}_n(t)$ may be evaluated by the inverse relation

$$\hat{u}_n = \frac{2}{N\bar{c}_n}\sum_{j=0}^{N}\frac{1}{\bar{c}_j}u_j(\xi_j,t)\cos(nj\pi/N), \tag{12}$$

where

$$\bar{c}_j = \begin{cases} 2, & j = 0,N \\ 1, & j = 1,2,\ldots,N-1. \end{cases} \tag{13}$$

The Chebyshev collocation spectral method can be seen as a technique of interpolation, thus Eq. (11) can be expressed in terms of the Lagrange polynomials. The Lagrange polynomials for the Chebyshev-Gauss-Lobatto points may be represented by the expression

$$g_j(\xi) = \frac{(-1)^{j+1}(1-\xi^2)T'_N(\xi)}{\bar{c}_j N^2(\xi-\xi_j)}, \quad j = 0,\ldots,N. \tag{14}$$

The differentiation step can be accomplished in the transformed space (the transform method) or in the physical space (the matrix multiplication method). The first method is performed efficiently by means of a fast cosine transform with a recurrence relation in the spectral space and the second method is based on the explicit expressions obtained by differentiating the Lagrange polynomials. The matrix multiplication method is used in this study because it is efficient and easy to implement.

The spatial derivative of $u(\xi,t)$ at the collocation points ξ_k is evaluated using the analytical derivative of the Lagrange polynomials

$$u^{(r)}(\xi_k) = \sum_{j=0}^{N} D_{kj}^{(r)}u(\xi_j), \quad r = 1,2,\ldots, \tag{15}$$

where $D_{kj}^{(r)} = g_j^{(r)}(\xi_k)$ are the elements of Chebyshev collocation derivative matrix and r is the order of differentiation. The

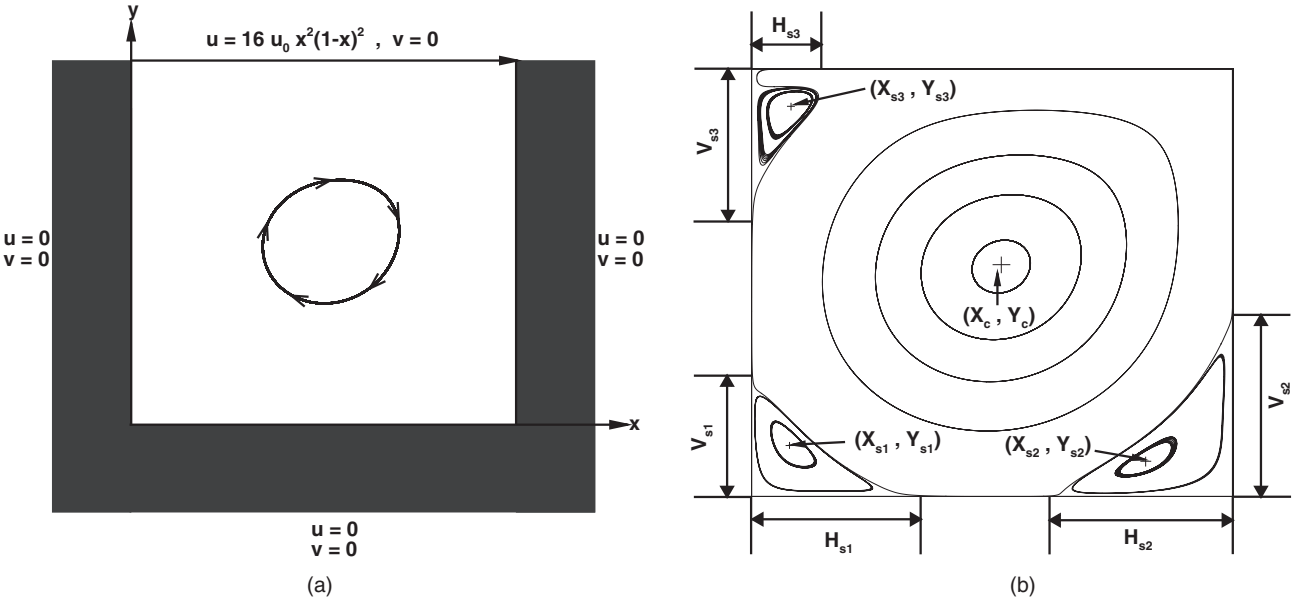

FIG. 3. The 2D regularized cavity flow: (a) boundary conditions and (b) flow configuration and nomenclature (see also Ref. [60]).

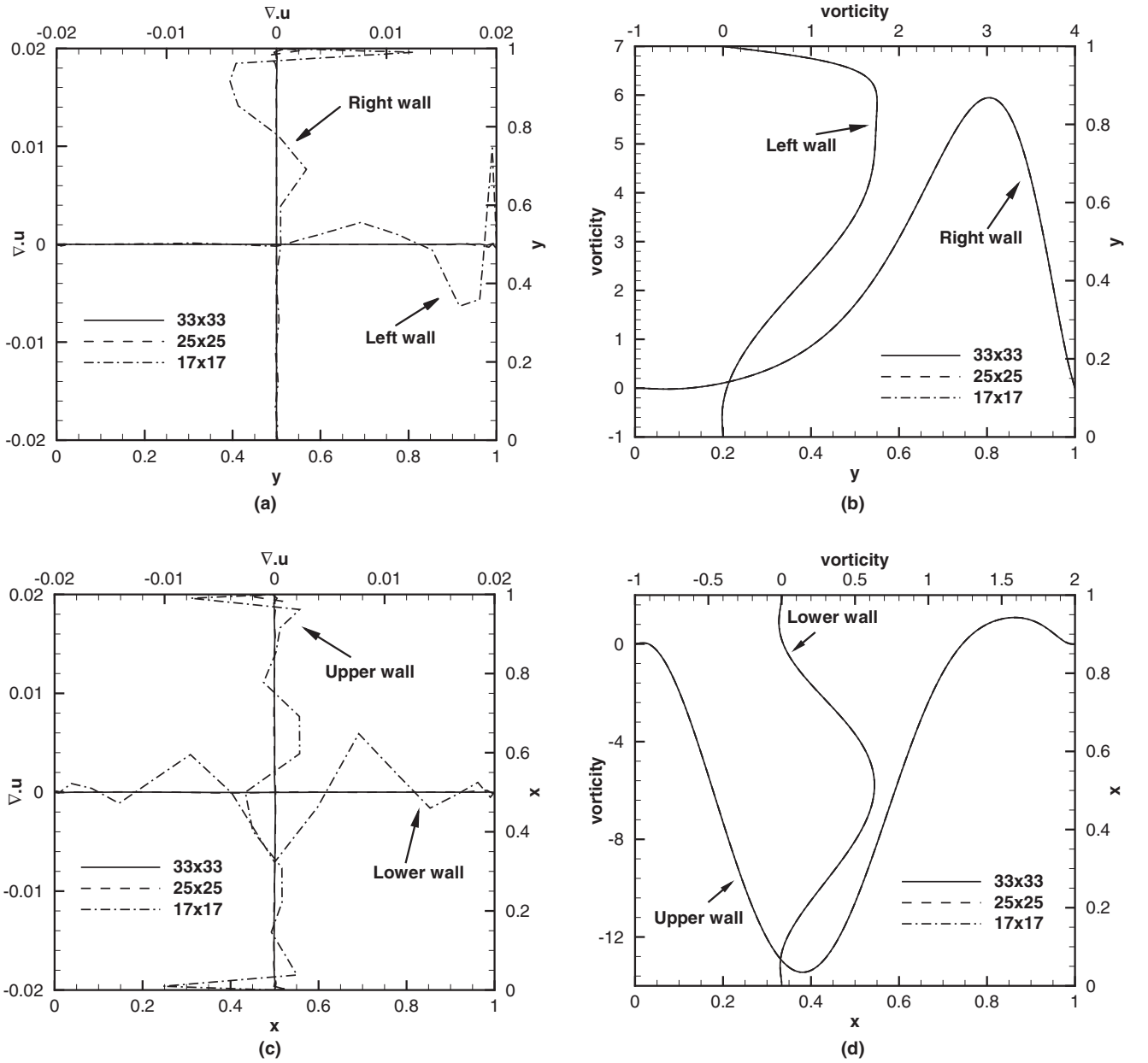

FIG. 4. Effect of grid size on (a) and (c) local compressibility and (b) and (d) vorticity for the 2D regularized cavity at Re = 100 for the (a) and (b) left and right walls and (c) and (d) upper and lower walls.

differentiation matrix $D^{(1)}_{kj}$ in a closed form is given by [55]

$$D^{(1)}_{kj} = \frac{c_k}{c_j}\frac{(-1)^{j+k}}{\xi_k - \xi_j}, \quad k \neq j$$
$$D^{(1)}_{kk} = -\frac{1}{2}\frac{\xi_k}{1-\xi_k^2}, \quad k \neq 0, N \tag{16}$$
$$D^{(1)}_{00} = -D^{(1)}_{NN} = \frac{2N^2+1}{6}.$$

The Chebyshev collocation second derivative matrix $D^{(2)}_{kj}$ can be obtained analytically using an explicit expression or by the relation $D^{(2)}_{kj} = (D^{(1)}_{kj})^2$.

Errors may be incurred when using the above analytic formula for calculating the differentiation matrices for the Chebyshev-Gauss-Lobatto points. In [51–53,56–58] it was explained that the error spoiling the first derivative is due to the roundoff error. An attempt was made in [58] to reduce the roundoff error by rewriting the elements of first derivative matrix as

$$D^{(1)}_{kj} = \begin{cases} \frac{\lambda_j}{\lambda_k}\frac{1}{\xi_k - \xi_j} & \text{for } k \neq j \\ -\sum_{i=0, i\neq k}^{N} \frac{\lambda_i}{\lambda_k}\frac{1}{\xi_k - \xi_i} & \text{for } k = j, \end{cases} \tag{17}$$

where

$$\lambda_k^{-1} = \prod_{i=0, i\neq k}^{N} (\xi_k - \xi_i), \tag{18}$$

TABLE I. Comparison of variables M_1 and M_2 for the 2D regularized cavity at Re = 100.

Grid	M_1 Present work	M_1 Ref. [60]	M_1 Ref. [61]	M_1 Ref. [62]	M_2 Present work	M_2 Ref. [60]	M_2 Ref. [61]	M_2 Ref. [62]
17 × 17	13.3506	13.3347	13.3467	13.3687	13.4509	13.4628	13.4476	13.4663
21 × 21	13.1760	13.1869	13.1759	13.1780	13.4440	13.4472	13.4441	13.4459
25 × 25	13.4225	13.4291	13.4226	13.4227	13.4446	13.4449	13.4446	13.4446
33 × 33	13.3422	13.3441	13.3423	13.3422	13.4446	13.4443	13.4448	13.4447
41 × 41	13.4433	13.4430			13.4446	13.4444	13.4447	

and the elements of the second derivative matrix as

$$D^{(2)}_{kj} = \begin{cases} 2D^{(1)}_{kj}\left(D^{(1)}_{kk} - \frac{1}{\xi_k - \xi_j}\right) & \text{for } k \neq j \\ 2\left(D^{(1)}_{kk}\right)^2 + 2\sum_{i=0, i\neq k}^{N} D^{(1)}_{ki}\frac{1}{\xi_k - \xi_i} & \text{for } k = j. \end{cases} \quad (19)$$

In [51–53] it was mentioned that the above formulas are preferable to the other formulas when computing the elements of the first differentiation matrix for a higher number of grid points. Here these formulas are used for the calculation of

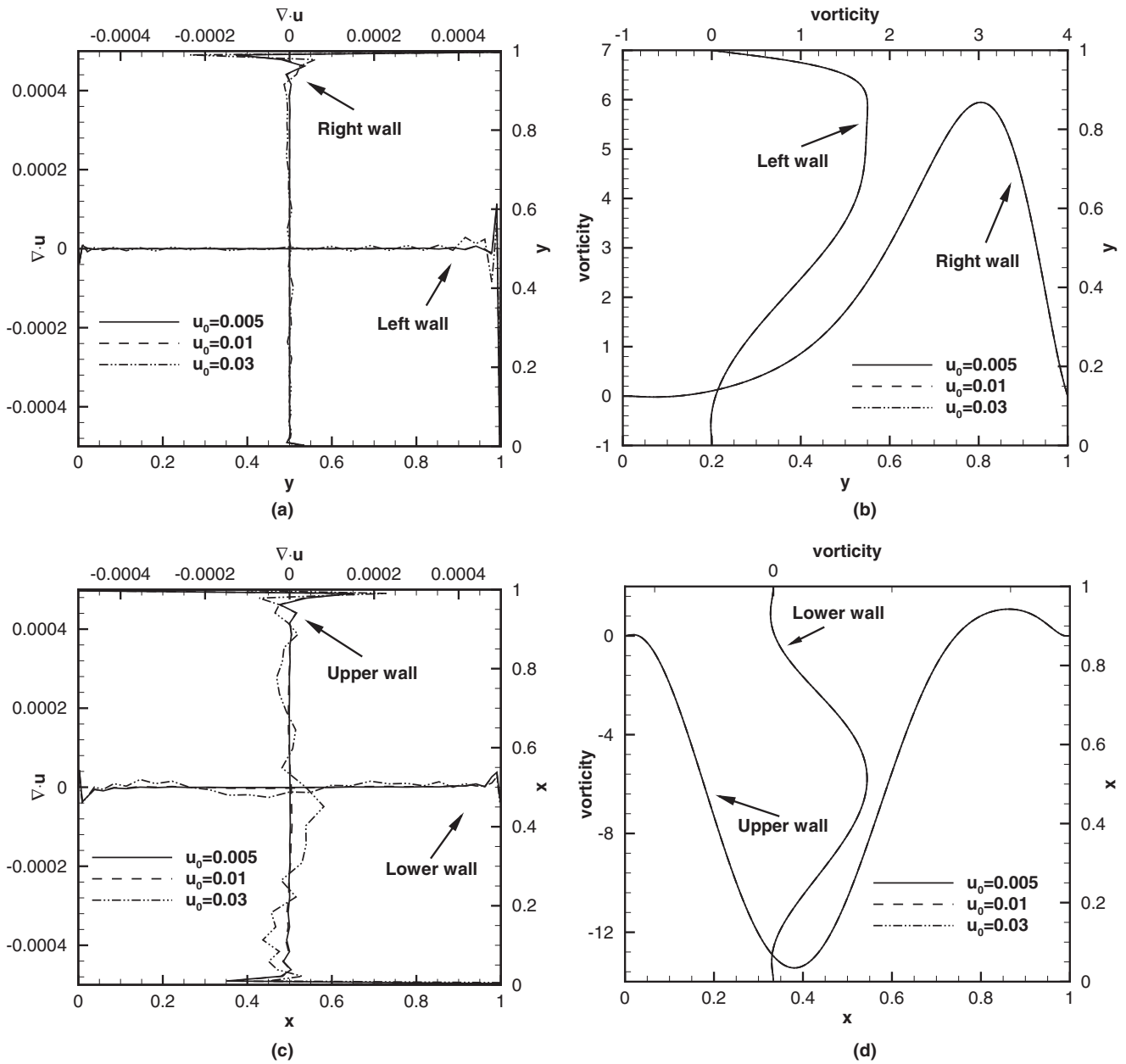

FIG. 5. Effect of value of characteristic velocity u_0 on (a) and (c) local compressibility and (b) and (d) vorticity for the 2D regularized cavity at Re = 100 at the (a) and (b) left and right walls and (c) and (d) upper and lower walls.

TABLE II. Comparison of variables M_1 and M_2 for the 2D regularized cavity at Re = 400.

Grid	M_1 Present work	M_1 Ref. [60]	M_1 Ref. [61]	M_1 Ref. [62]	M_2 Present work	M_2 Ref. [60]	M_2 Ref. [61]	M_2 Ref. [62]
17 × 17	24.9860	24.7189	24.7799	25.2329	25.2104	25.0855	25.1604	25.4675
21 × 21	24.6717	24.6189	24.6268	24.6693	24.9720	24.9362	24.9273	24.9846
25 × 25	24.9167	24.9172	24.9157	24.9344	24.9157	24.9176	24.9148	24.9333
33 × 33	24.7844	24.7821	24.7845	24.7845	24.9107	24.9110	24.9111	24.9110
41 × 41	24.8627	24.8622			24.9110	24.9108	24.9109	

the differentiation matrices. The procedure of rewriting the differentiation matrices ensures that the results obtained by applying the Chebyshev collocation spectral method are free of the roundoff error if used for a fine grid, without affecting the solution for a coarse grid.

The computational domain $\xi = [-1,1]$ is mapped to the physical domain $x = [a,b]$ by the simple transformation

$$x = \frac{a-b}{2}\xi + \frac{a+b}{2} \tag{20}$$

TABLE III. Comparison of values of flow characteristics for the 2D regularized cavity [see Fig. 3(b)] with different Re.

Re	Parameter	Present work	Grid	Ref. [60]	Grid	Ref. [46]	Grid
100	(x_c, y_c)	(0.603, 0.751)	33 × 33	(0.607, 0.753)	33 × 33	(0.609, 0.750)	17 × 17
	(x_{s1}, y_{s1})	(0.032, 0.032)		(0.032, 0.032)		(0.031, 0.031)	
	(x_{s2}, y_{s2})	(0.955, 0.047)		(0.955, 0.052)		(0.953, 0.047)	
	(H_{s1}, V_{s1})	(0.084, 0.084)		(0.130, 0.140)			
	(H_{s2}, V_{s2})	(0.114, 0.122)		(0.140, 0.140)			
400	(x_c, y_c)	(0.578, 0.617)	33 × 33	(0.578, 0.615)	33 × 33	(0.578, 0.625)	17 × 17
	(x_{s1}, y_{s1})	(0.045, 0.042)		(0.045, 0.041)		(0.031, 0.047)	
	(x_{s2}, y_{s2})	(0.902, 0.112)		(0.900, 0.115)		(0.922, 0.094)	
	(H_{s1}, V_{s1})	(0.113, 0.101)		(0.135, 0.110)			
	(H_{s2}, V_{s2})	(0.232, 0.292)		(0.250, 0.315)			
1000	(x_c, y_c)	(0.542, 0.573)	33 × 33	(0.545, 0.575)	33 × 33	(0.547, 0.578)	25 × 25
	(x_{s1}, y_{s1})	(0.076, 0.066)		(0.077, 0.068)		(0.078, 0.063)	
	(x_{s2}, y_{s2})	(0.875, 0.116)		(0.876, 0.118)		(0.922, 0.094)	
	(H_{s1}, V_{s1})	(0.203, 0.154)		(0.205, 0.170)			
	(H_{s2}, V_{s2})	(0.289, 0.349)		(0.320, 0.335)			
2000	(x_c, y_c)	(0.530, 0.553)	33 × 33	(0.535, 0.555)	33 × 33	(0.531, 0.547)	33 × 33
	(x_{s1}, y_{s1})	(0.090, 0.090)		(0.090, 0.090)		(0.094, 0.094)	
	(x_{s2}, y_{s2})	(0.856, 0.104)		(0.856, 0.107)		(0.922, 0.094)	
	(x_{s3}, y_{s3})	(0.032, 0.889)		(0.028, 0.888)		(0.031, 0.908)	
	(H_{s1}, V_{s1})	(0.260, 0.201)		(0.255, 0.195)			
	(H_{s2}, V_{s2})	(0.350, 0.385)		(0.350, 0.350)			
	(H_{s3}, V_{s3})	(0.050, 0.208)		(0.050, 0.140)			
5000	(x_c, y_c)	(0.519, 0.538)	49 × 49	(0.518, 0.543)	33 × 33	(0.516, 0.531)	33 × 33
	(x_{s1}, y_{s1})	(0.079, 0.123)		(0.081, 0.121)		(0.094, 0.094)	
	(x_{s2}, y_{s2})	(0.816, 0.082)		(0.818, 0.081)		(0.922, 0.094)	
	(x_{s3}, y_{s3})	(0.084, 0.910)		(0.082, 0.910)		(0.078, 0.908)	
	(H_{s1}, V_{s1})	(0.312, 0.253)		(0.350, 0.270)			
	(H_{s2}, V_{s2})	(0.359, 0.422)		(0.370, 0.415)			
	(H_{s3}, V_{s3})	(0.130, 0.298)		(0.130, 0.260)			
8000	(x_c, y_c)	(0.516, 0.533)	81 × 81				
	(x_{s1}, y_{s1})	(0.070, 0.141)					
	(x_{s2}, y_{s2})	(0.795, 0.070)					
	(x_{s3}, y_{s3})	(0.095, 0.918)					
	(H_{s1}, V_{s1})	(0.332, 0.274)					
	(H_{s2}, V_{s2})	(0.378, 0.440)					
	(H_{s3}, V_{s3})	(0.171, 0.332)					

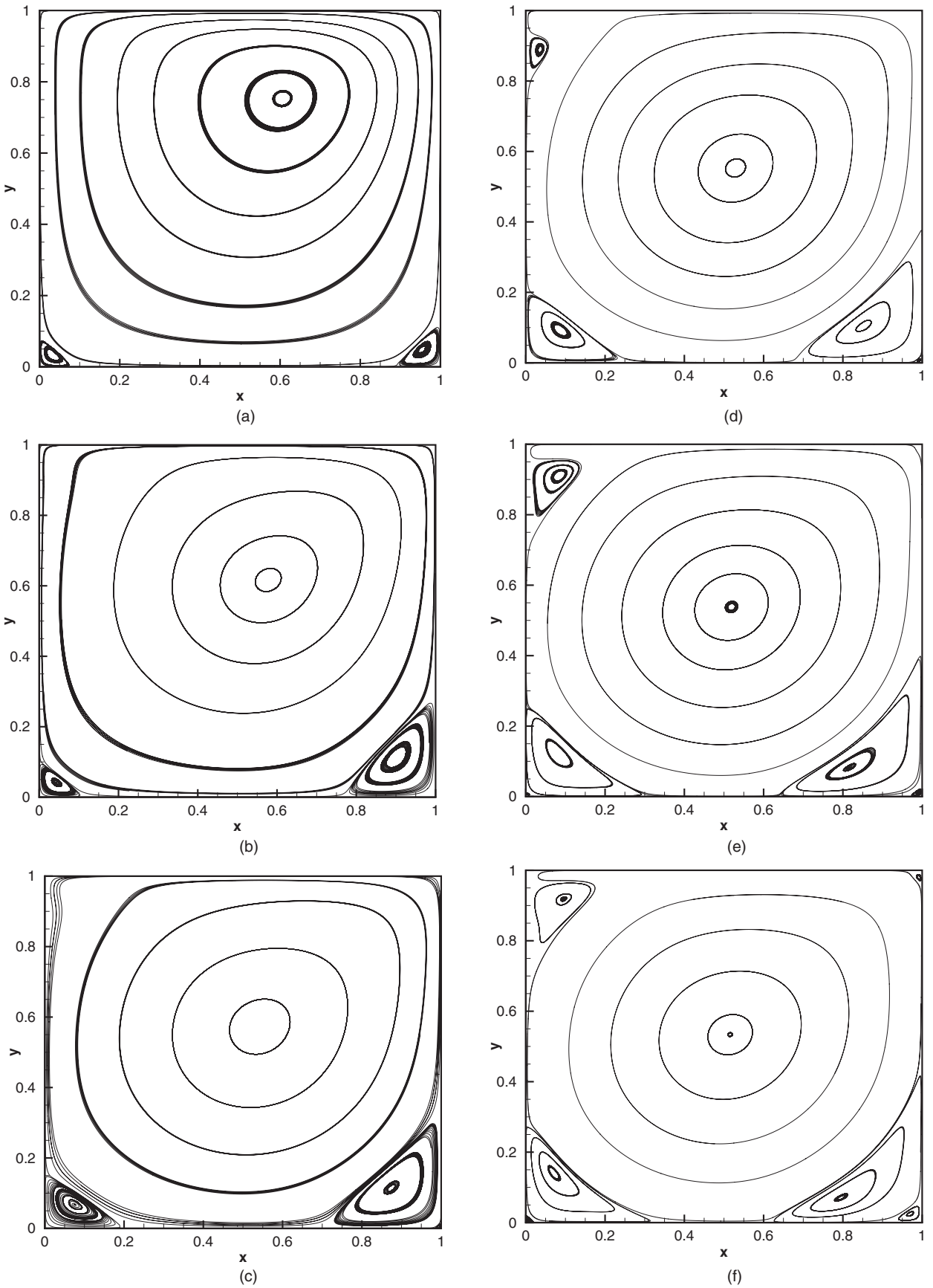

FIG. 6. Computed flow field for the 2D regularized cavity shown by streamlines at (a) Re = 100, (b) Re = 400, (c) Re = 1000, (d) Re = 2000, (e) Re = 5000, and (f) Re = 8000.

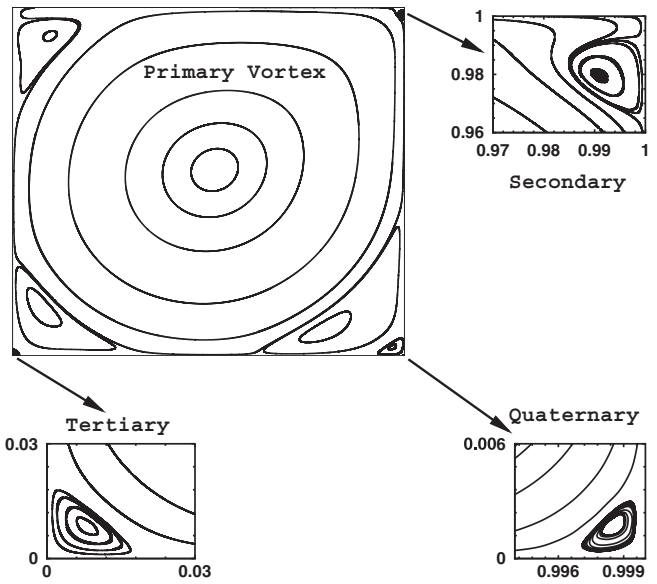

FIG. 7. Computed flow field for the 2D regularized cavity shown by streamlines at Re = 8000.

and therefore the differentiation matrices are expressed as

$$D^{(1)}_{kj}(x) = \left[D^{(1)}_{kj}(\xi)\right]\left(\frac{2}{a-b}\right),$$
$$D^{(2)}_{kj}(x) = \left[D^{(2)}_{kj}(\xi)\right]\left(\frac{2}{a-b}\right)^2. \tag{21}$$

The procedure given above for the calculation of the derivatives in one dimension can be readily extended to two dimensions. If an unknown matrix U is defined as $U(x_i, y_j) = u_{ij}$, then its partial derivatives evaluated at the collocation points can be expressed in terms of the matrix-matrix products, where the differentiation with respect to x corresponds to multiplying the rows of D_x (the collocation derivative matrix in the x direction) by the columns of U, and the differentiation with respect to y corresponds to multiplying the rows of U by the columns of D_y^T (the collocation derivative matrix transpose in the y direction).

Now, by performing the space discretization using the spectral method, the LB equation (2) can be written in the form

$$\frac{\partial f_k}{\partial t} = R_k, \tag{22}$$

where

$$R_{k_{m,n}} = -\left(e_{kx}\sum_{i=0}^{N_x} D_{x_{m,i}}\, f_{k_{i,n}} + e_{ky}\sum_{i=0}^{N_y} D^T_{y_{i,n}}\, f_{k_{m,i}}\right) - \frac{1}{\tau}\left(f_{k_{m,n}} - f^{eq}_{k_{m,n}}\right), \tag{23}$$

where m and n indicate the grid number in the x and y directions, respectively, D_x is the derivative matrix in the x direction, and D_y^T is the transpose of the collocation derivative matrix in the y direction. In addition, N_x and N_y are the polynomial degrees in each direction.

The discretization of the temporal term in Eq. (22) is performed by an explicit multistage time-stepping method. Here the solution is advanced in the time t by using the fourth-order Runge-Kutta scheme as follows:

$$\begin{aligned} f_k^0 &= f_k^t, \\ f_k^1 &= f_k^0 + \frac{\Delta t}{4} R_k^0, \\ f_k^2 &= f_k^0 + \frac{\Delta t}{3} R_k^1, \\ f_k^3 &= f_k^0 + \frac{\Delta t}{2} R_k^2, \\ f_k^{t+\Delta t} &= f_k^0 + \Delta t\, R_k^3. \end{aligned} \tag{24}$$

This time integration scheme is appropriate for an accurate simulation of unsteady flows.

IV. INITIALIZATION PROCEDURE

For the numerical solution of the lattice Boltzmann equation for low-speed flows, appropriate initialization of the distribution function f_k is required. The conventional procedure is to initialize the distribution function f_k by the equilibrium distribution function f_k^{eq} calculated based on the initial conditions of the macroscopic variables. This procedure is suitable for the solution of steady flows; however, some possible errors can be raised in the simulation of unsteady flows due to inconsistent initial conditions. An iterative procedure for generating consistent initial conditions for the LB equation, based on the density as the conserved variable with a given velocity field, has been proposed by Mei *et al.* [59]. In the present study, an iterative procedure is used based on the CCSLBM to provide consistent initial conditions for the distribution function f_k by calculating the pressure as the conserved variable with a given velocity field. Such a procedure has been suggested and applied in [44] to provide suitable initial conditions for unsteady low-speed flows by implementing the high-order compact finite-difference LBM (the CFDLBM). For this purpose, the following subsequent steps are used in this procedure.

(i) The equilibrium distribution function f_k^{eq} is calculated based on the initial velocity and pressure field by Eq. (4).

(ii) The distribution function f_k is calculated by Eq. (24) with the Chebyshev collocation spectral method.

(iii) The pressure field is updated by Eq. (5) only, while the velocity field is fixed at the initial values.

(iv) The process is repeated until the pressure field converges within a specified criterion.

By applying this iterative process, the distribution function f_k and the pressure are calculated in the field that is consistent with the given initial velocity field. This iterative procedure is verified by solving the Taylor vortex problem (see Sec. VI).

V. BOUNDARY CONDITIONS

In general, the solution of spectral methods is sensitive to the boundary treatment and the algorithm may be unstable due to reflections of the numerical waves or errors from the boundaries into the flow field. Thus, the boundary conditions

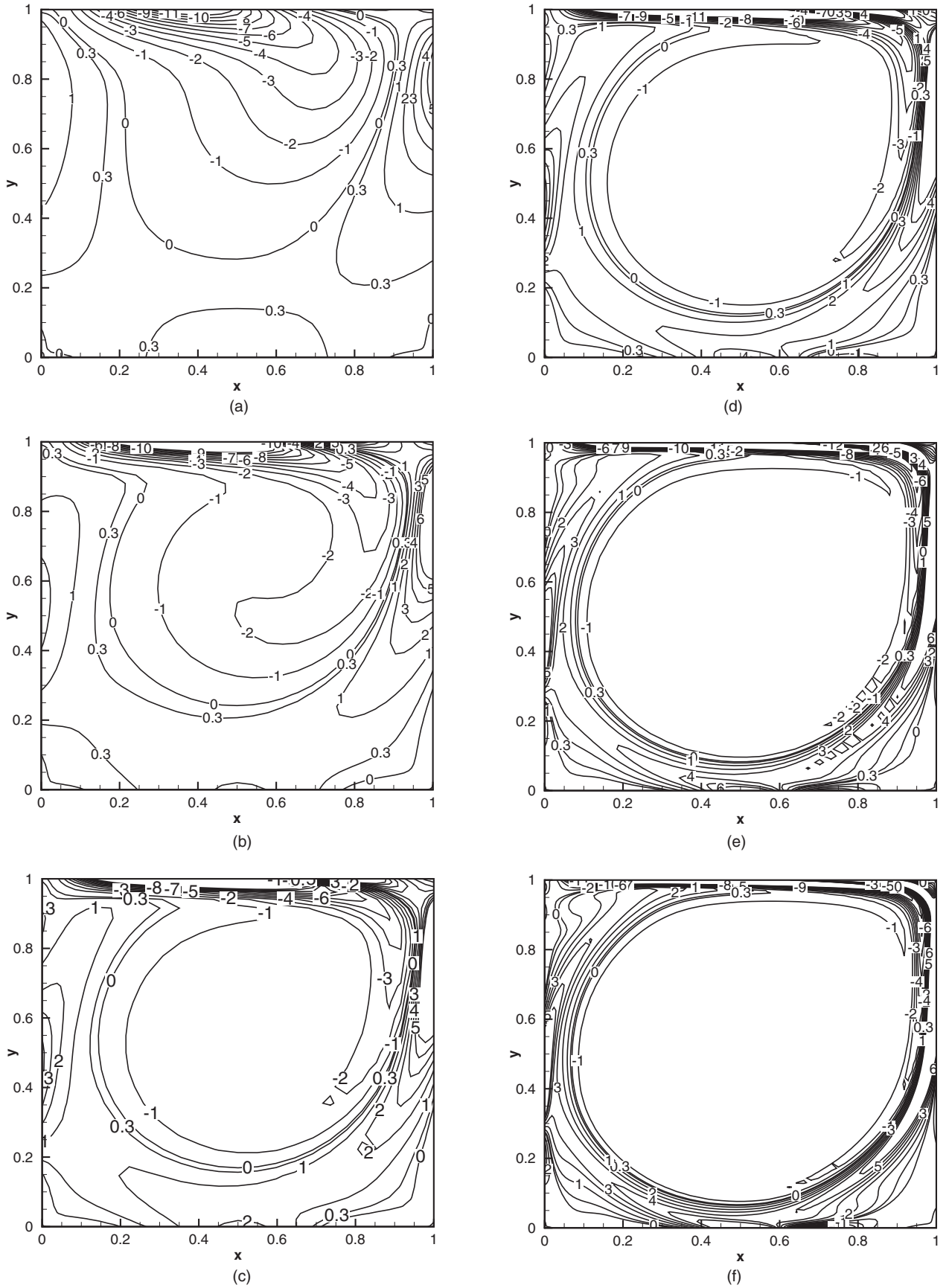

FIG. 8. Computed flow field shown by vorticity contours for the 2D regularized cavity at (a) Re = 100, (b) Re = 400, (c) Re = 1000, (d) Re = 2000, (e) Re = 5000, and (f) Re = 8000.

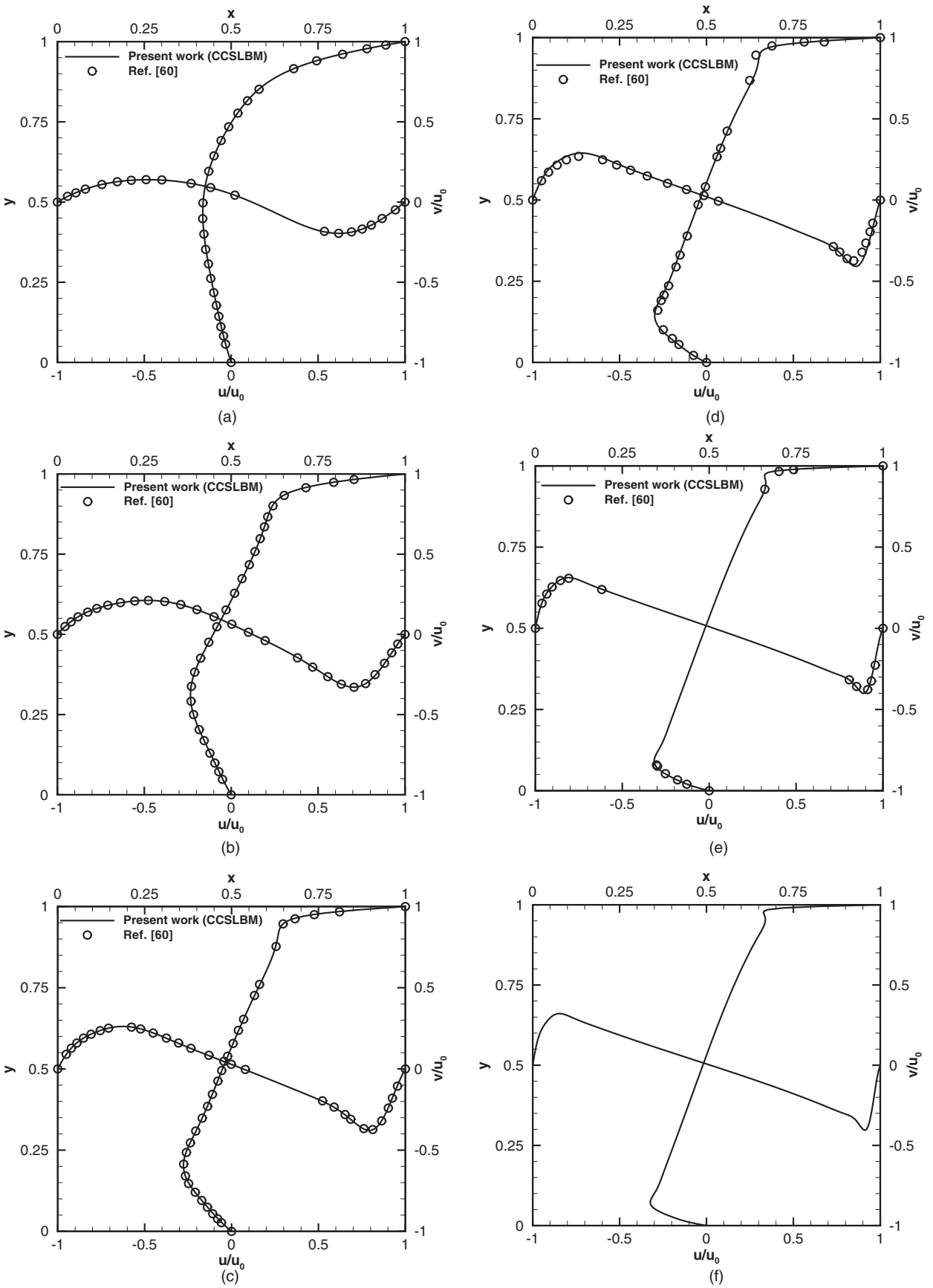

FIG. 9. Comparison of velocity profiles at midplanes of the 2D regularized cavity at (a) Re = 100, (b) Re = 400, (c) Re = 1000, (d) Re = 2000, Re = 5000, and (f) Re = 8000.

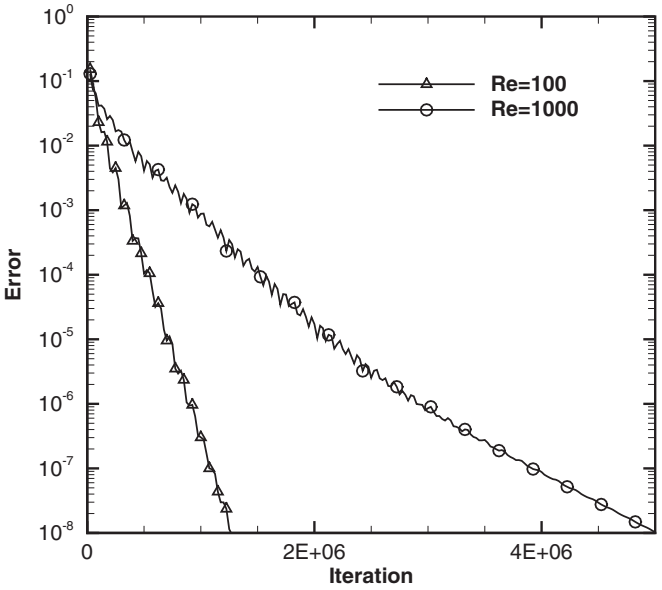

FIG. 10. Convergence history of the solution for the 2D regularized cavity flow with Re = 100 and 1000.

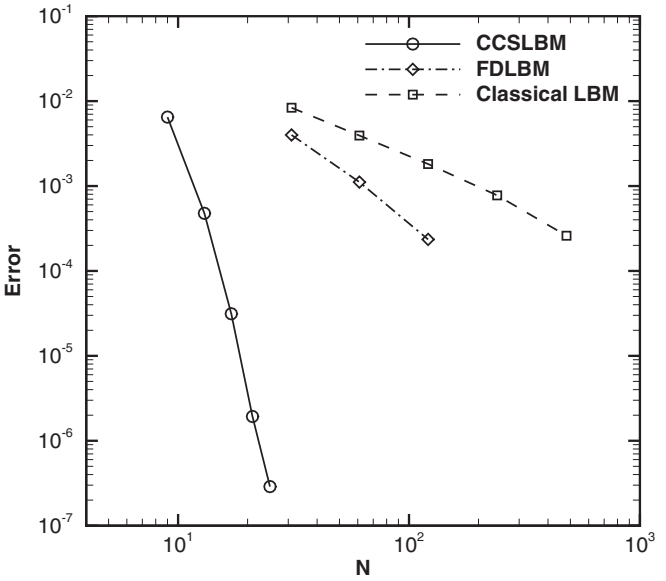

FIG. 11. Comparison of the L_2-norm error of the solution for the 2D regularized cavity at Re = 100 obtained by the CCSLBM with the FDLBM and the classical LBM.

for spectral methods should be implemented in a way to avoid reflections of these numerical errors.

The Chebyshev collocation spectral method applied to solve the LB equation needs suitable boundary conditions for both the macroscopic and microscopic variables. In the LB equation, the distribution function f_k is not given directly at the boundaries and a special treatment should be utilized for determining its value based on the macroscopic variables on each boundary. Here the approach is to use physical boundary conditions based on the solution of the governing equations implemented on the boundaries. On a wall boundary with the no-slip condition, the values of the macroscopic velocity components are known at each time step. To calculate the pressure on a wall boundary, one can obtain the following physical formula by employing the momentum equations at the wall:

$$\frac{\partial p}{\partial y_n} = \mu \frac{\partial^2 u_n}{\partial y_n^2}, \tag{25}$$

where y_n indicates the distance in the wall-normal direction and u_n is the normal velocity with respect to the boundary. By implementing the Chebyshev collocation spectral method in Eq. (25), for example, the wall boundaries $x = 0$ and $x = L$, the pressure values at these two walls $p_{0,n}$ and $p_{N_x,n}$ can be calculated simultaneously by the relations

$$D^{(1)}_{0,0} p_{0,n} + \sum_{i=1}^{N_x-1} D^{(1)}_{0,i} p_{i,n} + D^{(1)}_{0,N_x} p_{N_x,n} = \mu \sum_{i=0}^{N_x} D^{(2)}_{0,i} u_{i,n}, \tag{26}$$

$$D^{(1)}_{N_x,0} p_{0,n} + \sum_{i=1}^{N_x-1} D^{(1)}_{N_x,i} p_{i,n} + D^{(1)}_{N_x,N_x} p_{N_x,n} = \mu \sum_{i=0}^{N_x} D^{(2)}_{N_x,i} u_{i,n}. \tag{27}$$

The same procedure can be used to calculate the pressure on the other boundaries. After updating the macroscopic variables, the equilibrium distribution function $f^{eq}(u,v,p)$ at the boundaries is also updated by its formula, Eq. (4). Then, to calculate the distribution function f_k at a new time step, Eq. (24) is solved at the boundaries with the same algorithm used for the interior points.

VI. NUMERICAL RESULTS FOR 2D PROBLEMS

Herein, both steady and unsteady low-speed flows are simulated by applying the CCSLBM. To verify the steady computations, a benchmark test case is considered: a 2D regularized driven cavity flow. The 2D cavity flow simulated here is a suitable problem to show that the CCSLBM is an effective solver to accurately compute steady flow problems with complex flow field structures and the solution methodology is robust and stable even at high Reynolds numbers. Results obtained for this problem by applying the CCSLBM are thoroughly compared and verified with those of the Chebyshev collocation spectral Navier-Stokes flow solvers. The Taylor vortex problem is simulated here to examine the accuracy of the solution algorithm for an unsteady simulation and also to assess the iterative solution procedure proposed for providing the required initial conditions. The doubly periodic shear layer problem is simulated here to show that the CCSLBM does not need any filtering for the solution to be stable, unlike the other LBM solvers. Results obtained from these cases are compared with the analytical solutions and the available numerical results.

To further assess the accuracy and performance of the CCSLBM, the present results are also compared with the standard streaming-collision (classical) LBM and two other finite-difference LBM solvers, namely, the fourth-order CFDLBM [44] and the developed second-order central FDLBM. Note that both these finite-difference LBM solvers require a filtering procedure to damp high-frequency oscillations associated with the central differencing of the spatial derivatives in the LB

TABLE IV. Comparison of error norms, CPU time, and memory usage for the solution of the 2D regularized cavity at Re = 100 obtained by the CCSLBM with the FDLBM and the classical LBM.

Grid	L_∞	L_2	CPU time (h)	Memory usage (kilobytes)
		CCSLBM		
9×9	1.8×10^{-2}	6.5×10^{-3}	0.20	864
13×13	1.5×10^{-3}	4.8×10^{-4}	0.27	880
17×17	1.1×10^{-4}	3.1×10^{-5}	0.44	960
21×21	6.6×10^{-6}	1.9×10^{-6}	0.63	992
25×25	3.1×10^{-6}	2.9×10^{-7}	0.84	1124
		FDLBM		
31×31	1.7×10^{-2}	4.0×10^{-3}	3.40	1216
61×61	5.4×10^{-3}	1.1×10^{-3}	12.67	1896
121×121	1.1×10^{-3}	2.35×10^{-4}	29.96	4792
		Classical LBM		
31×31	2.8×10^{-2}	8.4×10^{-3}	0.11	732
61×61	1.3×10^{-2}	3.9×10^{-3}	0.07	1280
121×121	5.9×10^{-3}	1.8×10^{-3}	0.53	3368
241×241	2.5×10^{-3}	7.8×10^{-4}	4.01	11400
481×481	1.2×10^{-3}	2.6×10^{-4}	30.89	43800

equation. The high-order implicit filtering technique applied for the CFDLBM [44] is also used for the stabilization of the developed FDLBM. All the calculations are performed on Intel core i7-3630QM 2.4-GHz processor with a 64-bit operating system (N46VZ laptop).

A. Steady flow in a two-dimensional regularized cavity

In order to show the high accuracy of the Chebyshev collocation spectral LBM proposed, a 2D regularized driven cavity flow is simulated. In this problem, the singularity at the upper corners is resolved using a parabolic horizontal velocity distribution instead of a constant velocity. The results presented are based on the Chebyshev-Gauss-Lobatto grid points of 17×17 up to 81×81 depending on the value of Reynolds numbers.

The regularized square driven cavity [see Fig. 3(a)] is a model for the flow in a cavity where the upper boundary moves to the right with the velocity distribution

$$\boldsymbol{u} = [u_0 16x^2(1-x)^2, 0] \tag{28}$$

and $\boldsymbol{u} = (0,0)$ on the other wall boundaries. The horizontal velocity distribution has a maximum velocity $u_{\max} = u_0$ and the Reynolds number is defined as $\mathrm{Re} = u_{\max} L_c/\upsilon$. The estimation of the error for the convergence study is based on the nondimensional vorticity variable defined as $\omega = \partial v/\partial x - \partial u/\partial y$ by the following criteria:

$$\frac{\sum_{i=1}^{N-1}\sum_{j=1}^{M-1}\left|\omega_{i,j}^{n+1} - \omega_{i,j}^{n}\right|}{\Delta t \sum_{i=1}^{N-1}\sum_{j=1}^{M-1}\left|\omega_{i,j}^{n+1}\right|} < \varepsilon = 10^{-8}. \tag{29}$$

At first, a sensitivity study is performed to examine the effects of the grid size and the value of characteristic velocity u_0 on the results obtained for the 2D regularized cavity by applying the CCSLBM. Figure 4 shows a grid refinement study on the local compressibility $\nabla \cdot \boldsymbol{u}$ and the vorticity on the cavity walls for Re = 100 using $u_0 = 0.03$. It is observed that by increasing the number of grid points, the level of local compressibility significantly decreases on all the walls and a more accurate solution is obtained. However, it is demonstrated that the physical variables, such as the vorticity, do not depend on the grid size for the grids used and the results are free of any oscillation. The maximum vorticity on the upper wall obtained by the present solution applying the CCSLBM is in agreement with the available numerical results obtained by the spectral Navier-Stokes solvers (see Table I). The effect of the value of characteristic velocity on the local compressibility error and the vorticity for all the cavity walls for the same Reynolds number considering the 33×33 grid is investigated in Fig. 5. It is shown that by selecting a smaller value of the characteristic velocity the compressibility error decreases on all the cavity walls and the incompressibility condition is nearly satisfied. Note that the level of the compressibility error close to the upper corners is slightly higher than other regions. The study indicates that the value of the characteristic velocity should be selected as small as possible to reduce the compressibility effect to provide reasonable results of incompressible flows. It is indicated that the value of the characteristic velocity does not significantly affect the vorticity on all the cavity walls.

Next the flow field characteristics obtained by applying the CCSLBM are compared with the other computations by applying the spectral methods [60–62]. Martinez and Esperanca [60] and Botella [61] used the Chebyshev collocation spectral method to solve the incompressible Navier-Stokes equations by using the projection method and Ehrenstein and Peyret [62] also applied the Chebyshev collocation spectral method to solve incompressible flows by the vorticity-stream function formulation. To compare the present computations with the available results, the variables M_1 and M_2, based on the study of Martinez and Esperance, are used in which

$$M_1 = \max|\omega(x_i,1)|, \quad x_i = \cos(i\pi/N_x), \quad i = 0,\ldots,N_x, \tag{30}$$

based on the collocation points, and

$$M_2 = \max|\omega(\tilde{x}_i,1)|, \quad \tilde{x}_i = -i/100 + 1, \quad i = 0,\ldots,200, \tag{31}$$

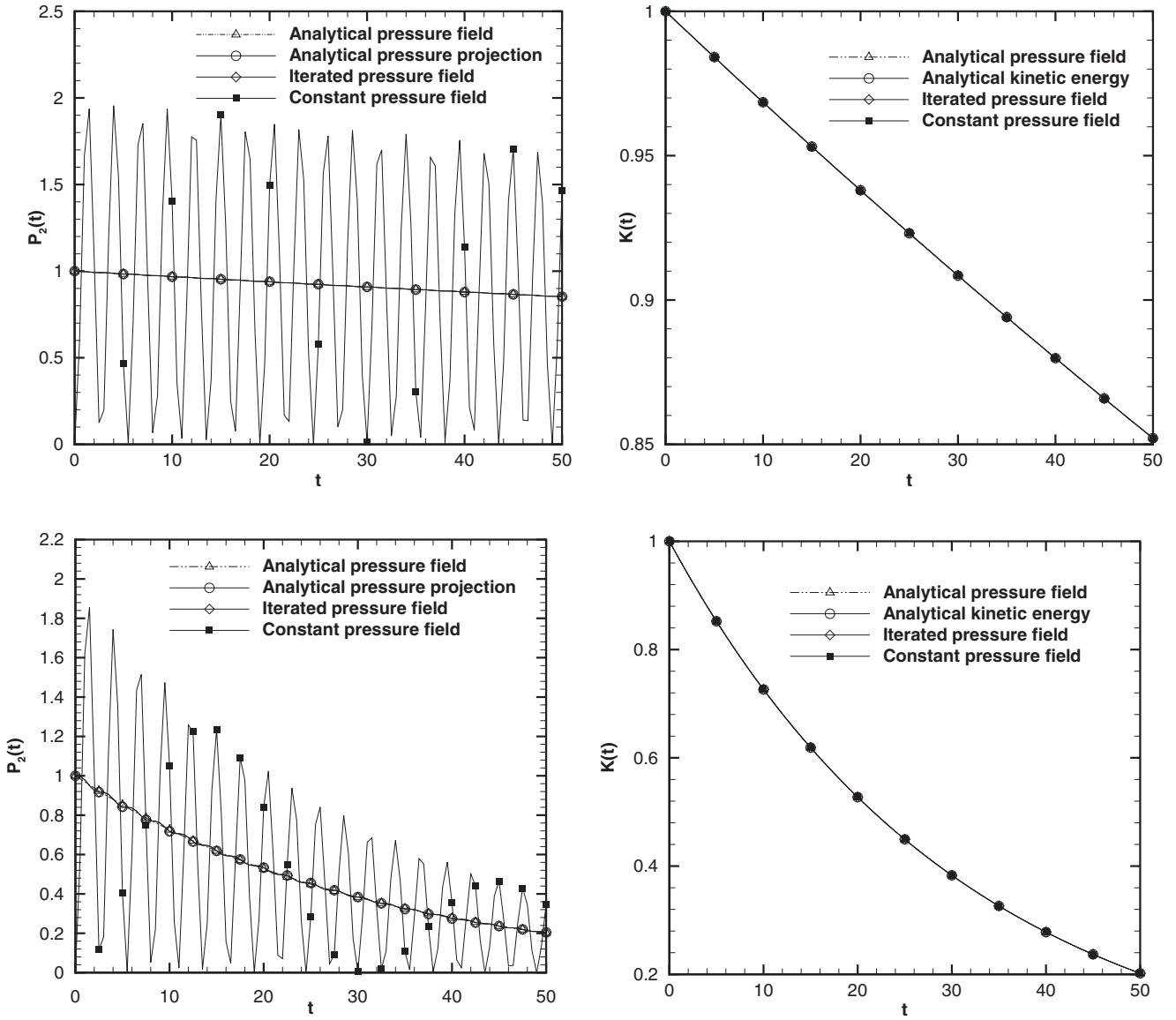

FIG. 12. Effect of different initial conditions for the pressure field on $P_2(t)$ (left) and $K(t)$ (right) for a grid size of 17×17 with $\upsilon = 0.0002$ (top) and $\upsilon = 0.002$ (bottom).

based on the interpolation of the solution on 201 equally spaced grid points where $\omega(\tilde{x}_i, 1)$ is reconstructed as

$$\omega(\tilde{x}_i,1) = \sum_{k=0}^{N_x} \frac{2}{\bar{c}_k N_x} \cos[k\cos^{-1}(\tilde{x}_i)] \times \left[\sum_{j=0}^{N_x} \frac{1}{\bar{c}_j} \omega(N_x - j, N_y) \cos\left(\frac{k\pi j}{N_x}\right) \right]. \quad (32)$$

Tables I and II display these comparisons for $\mathrm{Re} = 100$ and 400, respectively, and indicate that the present results for the values of M_1 and M_2 are in good agreement with those reported in [60–62]. When the spatial resolution N_x (the polynomial degree in the x direction) increases, the distribution of the Chebyshev-Gauss-Lobatto points changes. In contrast with M_1, the variable M_2 is implemented in a fixed distribution of the points when N_x increases. In Tables I and II it can be seen that M_2 gives a precise spectral convergence, which is not the case for M_1.

To accurately compute the flow field in the 2D regularized cavity, for Reynolds numbers up to 2000 a mesh of 33×33 and for $\mathrm{Re} = 5000$ and 8000 a mesh of 49×49 and 81×81, respectively, are used. Here the time step $\Delta t = \tau$ is adopted to obtain a stable solution at high-Reynolds-number flows. The locations of the center of the primary and secondary vortices are obtained by applying the Chebyshev collocation spectral LBM given in Table III and compared with the available numerical results [60,46]. The comparison is based on the nomenclature shown in Fig. 3(b). Shen [46] used the projection scheme in conjunction with a Chebyshev-Tau space discretization and his results are based on a mesh of 17×17 up to 49×49 depending on the Reynolds numbers (see Table III). The present results obtained by implementing

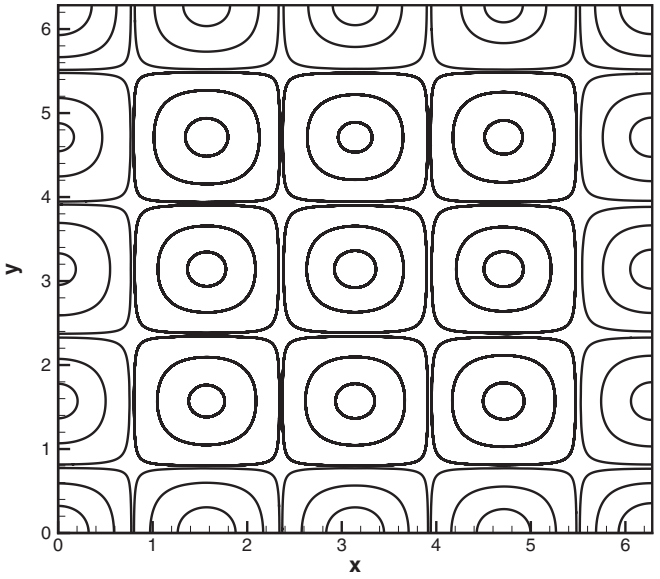

FIG. 13. Computed flow field for the Taylor vortex problem shown by streamlines with $\mathrm{Re} = u_0 L/\upsilon = 10\pi$ at $t^* = u_0 t/L = 1/20\pi$.

the Chebyshev collocation spectral LBM are in good agreement with those of Chebyshev collocation spectral Navier-Stokes flow solvers [60,46].

Figures 6(a)–6(f) give the steady-state results shown by the streamlines for the 2D regularized cavity for Reynolds numbers up to 8000. As the value of Re increases, the flow structure becomes more complex. Figure 7 shows that at $\mathrm{Re} = 8000$ the secondary, tertiary, and also quaternary vortices are well resolved, due to the condensed distribution of the Chebyshev-Gauss-Lobatto points near the boundary. The present study indicates that a quaternary corner vortex is observed in the flow field near the right-side region of the bottom wall at a steady-state solution. Figure 8 shows the

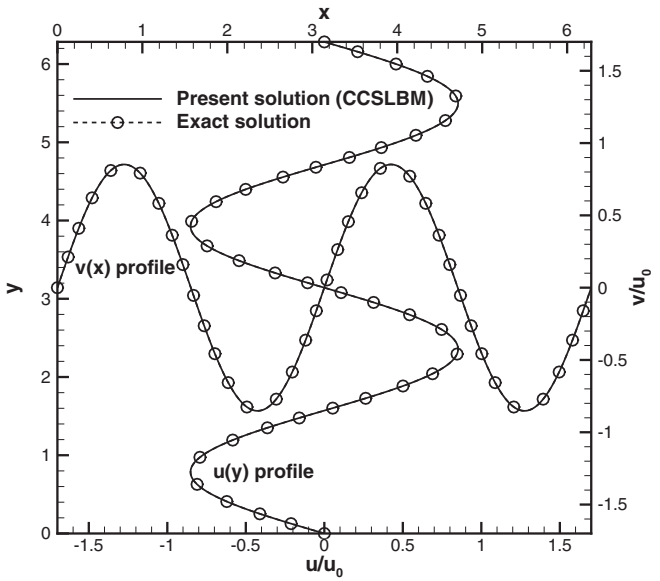

FIG. 14. Comparison of the u- and v-velocity profiles for the Taylor vortex problem with $\mathrm{Re} = u_0 L/\upsilon = 10\pi$ at $t^* = u_0 t/L = 1/20\pi$.

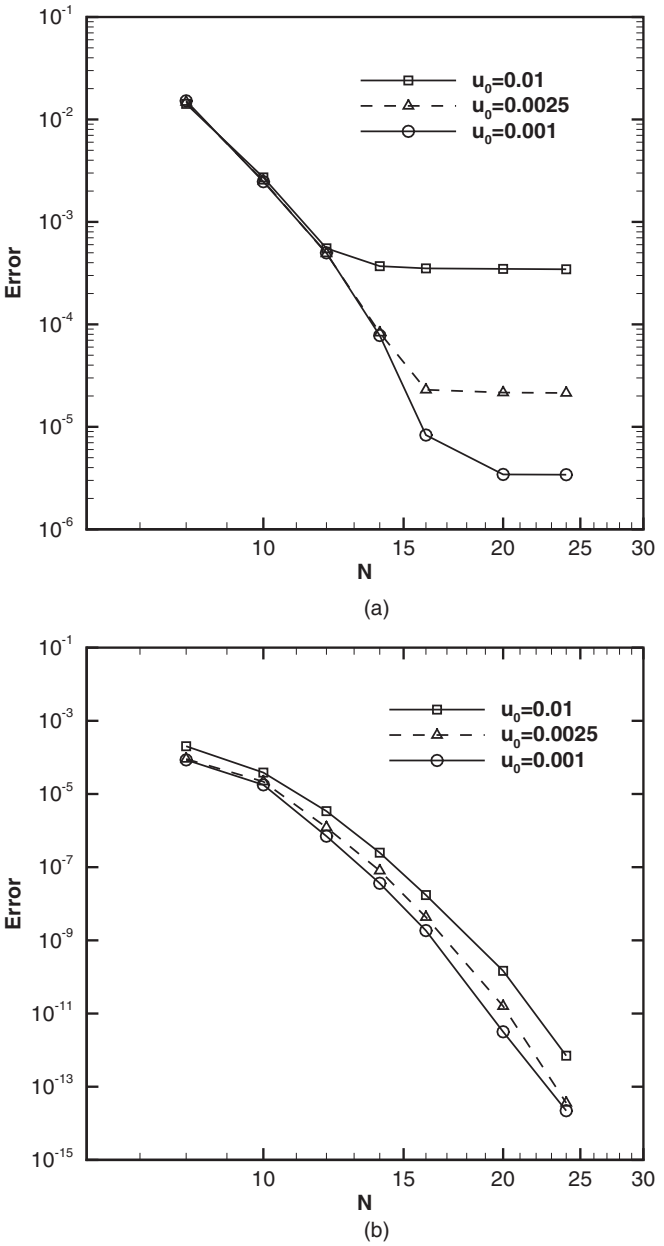

FIG. 15. Effect of the value of the characteristic velocity u_0 on the spectral convergence of the solution for the Taylor vortex problem for $\mathrm{Re} = u_0 L/\upsilon = 10\pi$ at $t^* = u_0 t/L = 1/(20\pi)$ based on L_2-norm error of solution compared with (a) the analytical solution (b) the most refined grid.

vorticity contours for the 2D regularized cavity flow at different Reynolds numbers. As the value of Re increases, the regions of high-vorticity gradients evolve and are shown by concentrating the vorticity contours. The u- and v-velocity profiles along the centerlines of the regularized cavity for Reynolds numbers up to 8000 computed by the CCSLBM are shown in Fig. 9 and when compared with those of Martinez and Esperanca [60] exhibit excellent agreement. Figure 10 illustrates the convergence history of the solution obtained by employing the CCSLBM based on the L_2 norm of the u-velocity profile in the flow field at $\mathrm{Re} = 100$ and 1000. For a higher Re, more iterations are needed for the solution to converge.

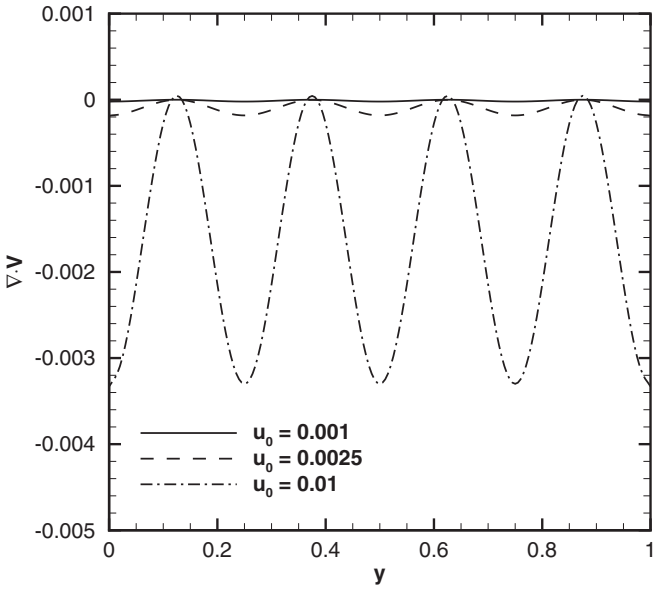

FIG. 16. Effect of the value of the characteristic velocity u_0 on the local compressibility error for the Taylor vortex problem for $\mathrm{Re} = u_0 L/\upsilon = 10\pi$ at $t^* = u_0 t/L = 1/20\pi$.

The computational efficiency of the proposed solution methodology based on the CCSLBM is examined by comparison with two other LBM solvers, namely, the standard collision-streaming (classical) LBM and the developed second-order central FDLBM. To do this the regularized cavity problem is investigated at $\mathrm{Re} = 100$ with $u_0 = 0.02$. Figure 11 shows a comparison of the L_2-norm error obtained by the CCSLBM with the classical LBM and the FDLBM. The L_2-norm error is defined based on the u-velocity profile in the entire flow field compared to the most refined grid. It is observed that the CCSLBM, when considering the same number of grid points, gives more accurate results than both the classical LBM and the FDLBM, and an exponential convergence is achieved rather than polynomial rates. The computational efficiency of the proposed solution methodology, the CCSLBM, in comparison with these two LBM solvers is shown in Table IV for the cavity problem at the same Re. As indicated, the CCSLBM reduces the CPU time and memory usage compared to both the classical LBM and the FDLBM when a high-accuracy solution is needed and the performance of the CCSLBM is highlighted in such conditions.

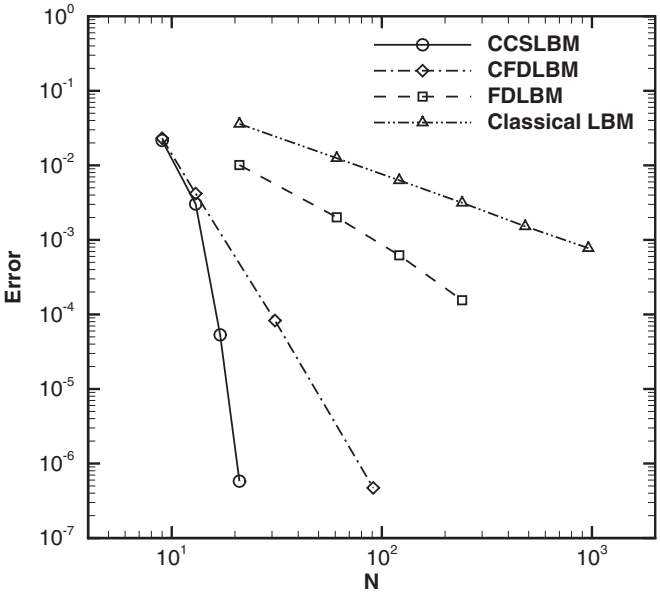

FIG. 17. Comparison of the L_2-norm error of the solution for the Taylor vortex problem for $\mathrm{Re} = u_0 L/\upsilon = 10\pi$ at $t^* = u_0 t/L = 1/5\pi$ obtained by the CCSLBM with the CFDLBM, the FDLBM, and the classical LBM.

B. The Taylor vortex problem

The Taylor vortex problem is solved to demonstrate the capability of the proposed CCSLBM for the unsteady calculations. This problem was introduced by Taylor [63] based on the incompressible Navier-Stokes equations in terms of the stream function-vorticity formulation. The exact solution for the velocity and pressure field for this problem is known as

$$u(x,y,t) = -u_0 \cos(k_x x)\sin(k_y y)e^{-k^2\upsilon t},$$
$$v(x,y,t) = \frac{k_x}{k_y} u_0 \cos(k_y y)\sin(k_x x)e^{-k^2\upsilon t},$$
$$p(x,y,t) = -\frac{1}{4}u_0^2\left[\cos(2k_x x) + \left(\frac{k_x}{k_y}\right)^2 \cos(2k_y y)\right]e^{-2k^2\upsilon t} + P_0, \quad (33)$$

where u_0 is the initial value of the characteristic velocity, υ is the kinematic viscosity, $k_x = 2\pi/L_x$ and $k_y = 2\pi/L_y$ are the wave numbers in the x and y directions, respectively, $k = \sqrt{k_x^2 + k_y^2}$, and P_0 is an arbitrary constant pressure (here $P_0 = 0$). Periodic boundary conditions are applied to all sides of the computational domain ($0 \leqslant x \leqslant L, 0 \leqslant y \leqslant L$, and $L = 2\pi$). The analytical initial conditions for the velocity and pressure field are obtained by setting $t = 0$ in Eq. (33).

Here $k_x = k_y = 2$ and the study is performed for two values of the kinematic viscosity $\upsilon = 0.0002$ and 0.002. The value of the characteristic velocity u_0 is set equal to 0.01 in this study unless otherwise specified. The normalized total kinetic energy $K(t)$,

$$K(t) = \frac{2}{4\pi^2 u_0^2}\int (u^2 + v^2)dxdy, \quad (34)$$

and the normalized projection of the pressure field $P_2(t)$,

$$P_2(t) = \frac{16}{4\pi^2 u_0^2}\int p(x,y,t) \times \cos[k_x(x+y)]\cos[k_y(x-y)]dxdy, \quad (35)$$

are compared for three different initialization schemes, including (a) using a constant pressure field for the initialization, (b) using the analytical solution of the pressure for the initialization, and (c) using the applied iterative scheme for the initialization.

Figure 12 shows the numerical results of $P_2(t)$ and $K(t)$ using the 17×17 grid for the two values of the kinematic viscosity $\upsilon = 0.002$ and 0.0002 and the analytical results are also given in this figure for the sake of comparison. From the plots $P_2(t)$, it can be seen that the initialized field considering a

TABLE V. Comparison of error norms, CPU time, and memory usage for the solution of the Taylor vortex problem obtained by the CCSLBM with the CFDLBM, the FDLBM, and the classical LBM.

Grid	L_∞	L_2	CPU time (h)	Memory usage (kilobytes)
		CCSLBM		
9×9	4.0×10^{-2}	2.2×10^{-2}	0.14	2752
13×13	5.2×10^{-3}	3.0×10^{-3}	0.31	2844
17×17	1.2×10^{-4}	5.3×10^{-5}	0.51	2956
21×21	1.6×10^{-6}	5.8×10^{-7}	0.93	3411
		CFDLBM		
9×9	4.4×10^{-2}	2.3×10^{-2}	0.03	1864
13×13	6.2×10^{-3}	4.2×10^{-3}	0.06	1884
31×31	1.2×10^{-4}	8.3×10^{-5}	0.37	2264
91×91	1.4×10^{-6}	4.7×10^{-7}	3.41	5648
		FDLBM		
21×21	4.8×10^{-2}	1.0×10^{-2}	0.91	2700
61×61	4.8×10^{-3}	2.0×10^{-3}	7.41	3580
121×121	1.2×10^{-3}	6.2×10^{-4}	29.26	6336
241×241	3.1×10^{-4}	1.65×10^{-4}	130.29	17500
		Classical LBM		
21×21	1.6×10^{-1}	3.6×10^{-2}	0.0016	548
61×61	5.4×10^{-2}	1.25×10^{-2}	0.04	1320
121×121	2.7×10^{-2}	6.3×10^{-3}	0.16	3620
241×241	1.4×10^{-2}	3.15×10^{-3}	1.01	12952
481×481	6.9×10^{-3}	1.5×10^{-3}	7.51	49100
961×961	3.6×10^{-3}	7.8×10^{-4}	69.02	194300

constant pressure value generates several acoustic oscillations due to the inaccurate initial condition. However, for the cases in which the pressure field is initialized by the analytical formula or by the iterative initialization procedure, there are no severe acoustic oscillations. It is observed that the total kinetic energy $K(t)$ is not affected by all the initialization schemes and there is no deficit between the calculated and analytical solutions. It can also be seen that the performance of the solution algorithm based on the CCSLBM is nearly the same for different values of kinematic viscosity υ and even for a small υ the solution obtained is stable without using a filtering procedure. Therefore, it can be concluded that by applying the iterative initialization procedure the CCSLBM can provide accurate unsteady solutions comparable with the analytical results.

Figure 13 shows the Taylor vortices for $\mathrm{Re} = u_0 L/\upsilon = 10\pi$ at $t^* = u_0 t/L = 1/20\pi$. The number of vortices is defined by $2k_x$ in each direction. The present computations obtained by the CCSLBM for the normalized velocity components $(u/u_0, v/u_0)$ at the midlines $y = \pi$ and $x = \pi$ employing the 17×17 grid are compared with the exact solution at $t^* = 1/20\pi$, as shown in Fig. 14, and exhibit excellent agreement. To verify the spectral convergence of the solution, different grid sizes, namely, 9×9, 11×11, 13×13, 15×15, 17×17, 21×21, and 25×25 are used. The error of the solution for this test case is shown in Fig. 15 and is calculated based on the L_2 norm of the u-velocity profile in two ways: (a) compared with the analytical solution and (b) compared with the most refined grid solution for $\mathrm{Re} = u_0 L/\upsilon = 2\pi$ at $t^* = 1/20\pi$. Here three different values of the characteristic velocity $u_0 = 0.01, 0.0025$, and 0.001 are used to investigate the effect of the value of the characteristic velocity on the accuracy of the solution. It is found that considering a small value for the characteristic velocity u_0 leads to a more accurate solution. In other words, a smaller characteristic velocity reduces the compressibility error (see Fig. 16 for the most refined 25×25 grid) and the exponential decay of the error and thus the spectral convergence can be achieved independent of the spatial resolution. When the error is calculated based on the most refined grid solution, it can be seen that the convergence depends on the value of the characteristic velocity.

The accuracy and performance of the present solution methodology are also examined for the Taylor vortex problem. This test case is computed for the characteristic velocity $u_0 = 0.001$ at the nondimensional time $t^* = u_0 t/L = 1/5\pi$. The L_2-norm error of the solution obtained by the CCSLBM is compared with the classical LBM, the FDLBM, and the CFDLBM, as shown in Fig. 17. The error is defined as the L_2 norm of the u-velocity profile in the entire flow field compared to the exact solution. It is illustrated that the CCSLBM for the same number of grid points gives more accurate results than the other LBM solvers. It is shown that the exponential convergence is achieved by the CCSLBM whereas other LBM solvers have a polynomial rate. Table V compares the performance of the CCSLBM with the classical LBM and the two finite-difference LBM solvers in terms of the CPU time and memory usage for the Taylor vortex problem. The error decays at an exponential rate when employing the CCSLBM, resulting in a lower number of grid points needed to provide a specified accuracy compared to the other LBM solvers. Table V indicates that when a high-accuracy solution is needed, the CCSLBM reduces the CPU time and memory usage compared to the other LBM methods.

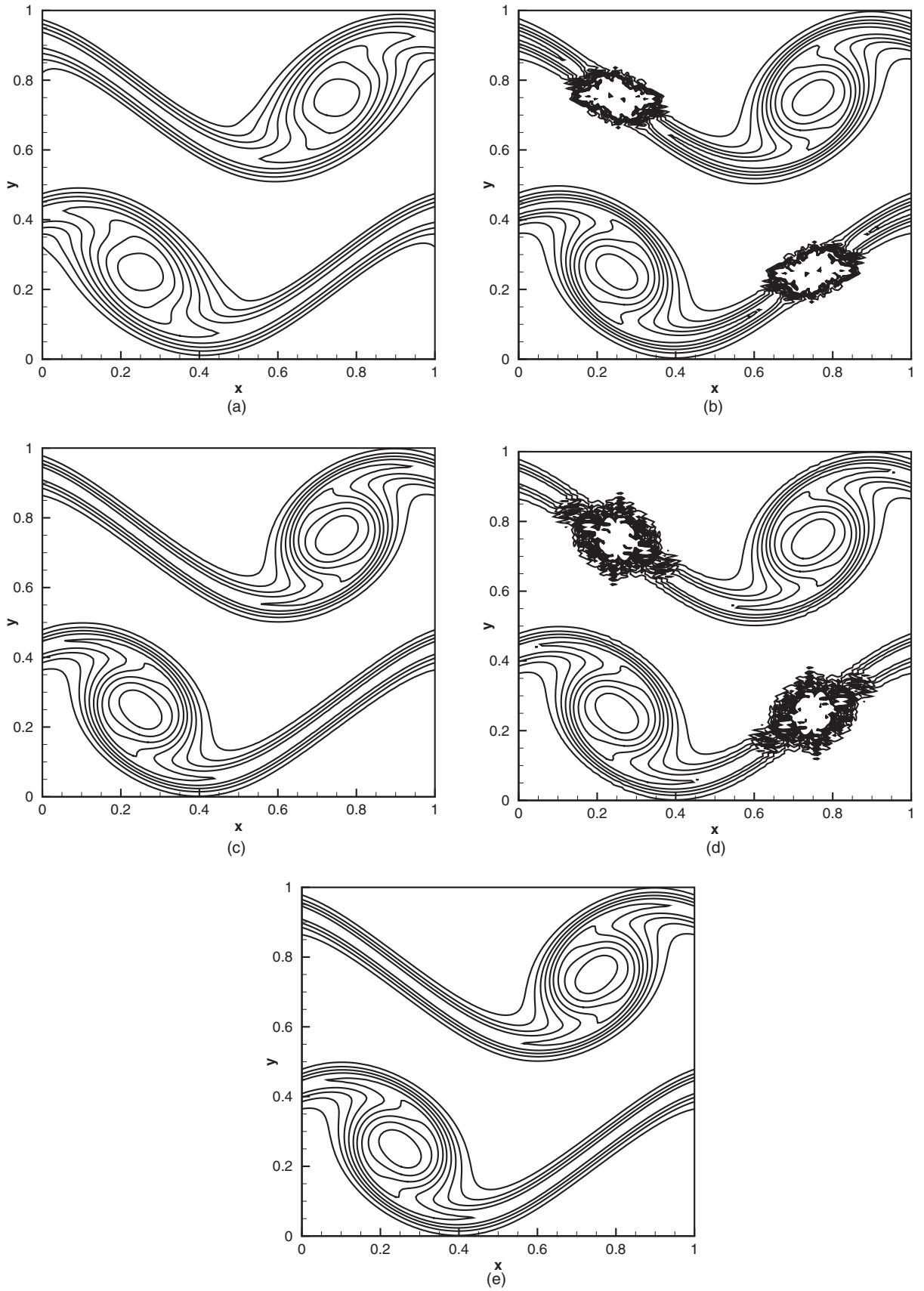

FIG. 18. Comparison of the vorticity contours for doubly periodic shear layers with $\upsilon = 0.0001$ at $t^* = 1$ obtained by the (a) and (b) FDLBM, with and without filtering, respectively; (c) and (d) CFDLBM, with and without filtering, respectively; and (e) CCSLBM, without filtering.

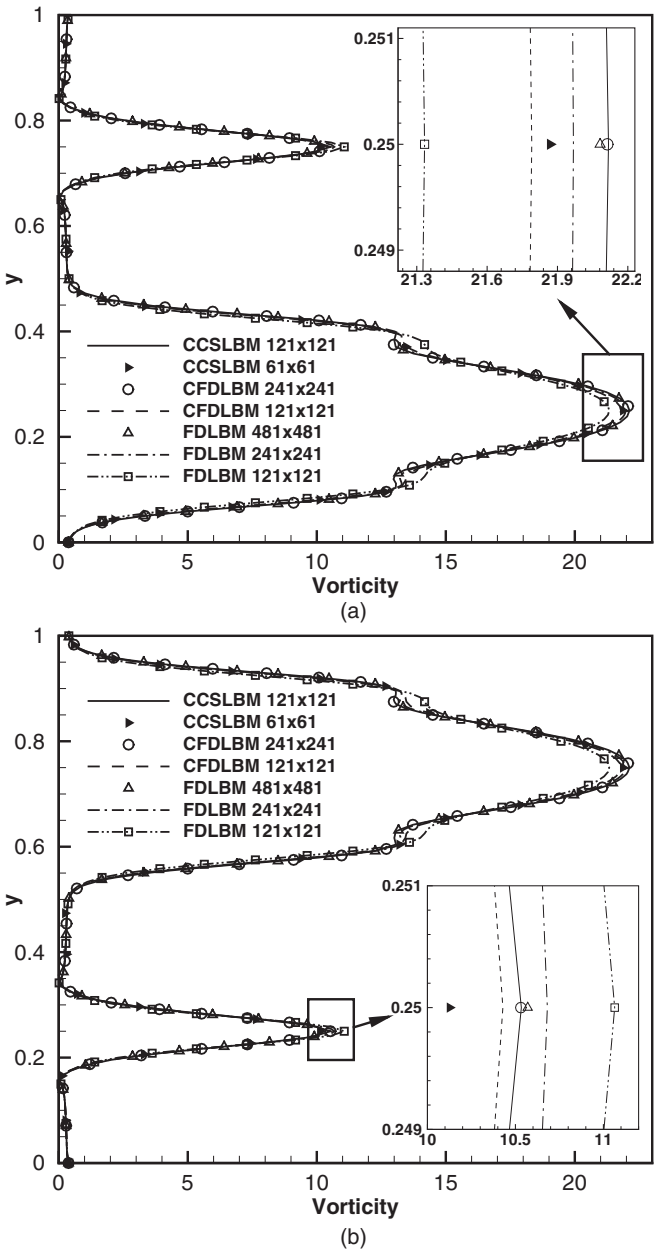

FIG. 19. Comparison of the vorticity profile at (a) $x = 0.25$ and (b) $x = 0.75$ for doubly periodic shear layers with $\upsilon = 0.0001$ at $t^* = 1$ obtained by the CCSLBM with the CFDLBM and the FDLBM.

C. Unsteady doubly periodic shear layers

The simulation of the unsteady doubly periodic shear flow problem [64,65] is performed to further assess the accuracy and robustness of the CCSLBM. In this problem, the initial conditions for the normalized velocity field are given by

$$\frac{u}{u_0} = \begin{cases} \tanh[4(y - 1/4)/w], & y \leqslant 1/2 \\ \tanh[4(3/4 - y)/w], & y > 1/2, \end{cases} \tag{36}$$

with $0 \leqslant x \leqslant 1$ and $0 \leqslant y \leqslant 1$, and

$$\frac{v}{u_0} = \delta \sin[2\pi(x + 1/4)],$$

where w approximates the initial shear layer width and δ is the strength of the initial perturbation. In this problem, the roll-up of the shear layer between the Kelvin-Helmholtz vortices is due to stretching. Simulations performed in the literature have shown that numerical instabilities may occur when the shear layers begin to roll up after several time steps and a special treatment should be applied to alleviate this problem when solving the LB equation [44,66]. The main advantage of applying the CCSLBM compared to the existing modes of solving the BGK formulation of the LB equation is that the proposed approach provides more accurate solutions and does not need any filtering, unlike other LBM solution procedures. To show this, the results obtained by applying the CCSLBM without filtering for the doubly periodic shear layer problem are compared with two other LBM solvers, namely, the CFDLBM [44] and the developed FDLBM with and without filtering. Here two computational grids, namely, 61×61 and 121×121, are used for the CCSLBM in the doubly periodic domain $0 \leqslant x, y \leqslant 1$ and the kinematic viscosity is set to be $\upsilon = 0.0001$. The perturbation parameter and the shear layer width are initialized by $\delta = 0.05$ and $w = 0.05$, respectively, and the value of u_0 is set equal to 0.1. Figure 18 illustrates the vorticity field for these LBM flow solvers at the nondimensional time $t^* = u_0 t/L = 1$. The implementation of the CCSLBM leads to a stable solution and the roll-up of the shear layers due to the Kelvin-Helmholtz vortices is accurately resolved. The stability of the solution without using a filtering procedure is clearly observed for solving this problem that has flow nonlinearities. Note that the two other LBM solvers require filtering for the solution to be stable. Figure 19 gives the vorticity profiles at two sections $x = 0.25$ and 0.75 at the same time predicted by the CCSLBM compared with these two finite-difference LBM solvers for a different number of grid points. This indicates that the CCSLBM with 121×121 grid points provides results

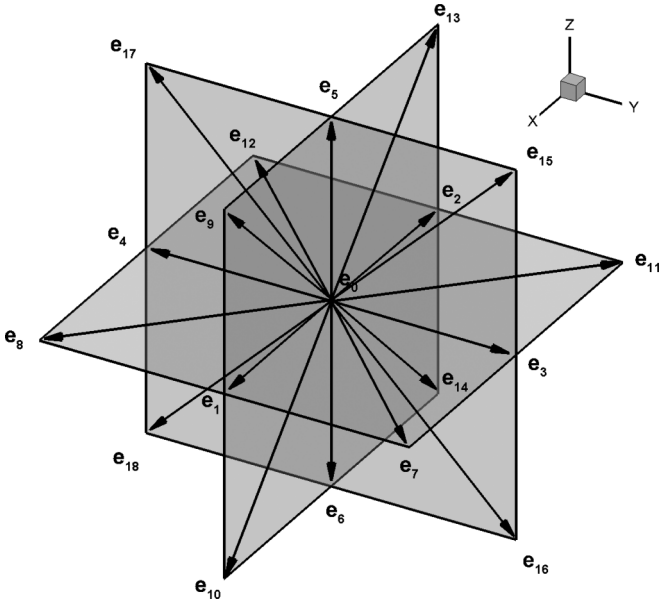

FIG. 20. The D3Q19 lattice and the microscopic velocities.

comparable to the CFDLBM and the FDLBM using 241×241 and 481×481 grid points, respectively.

VII. EXTENSION OF THE METHODOLOGY TO THREE DIMENSIONS

Here the formulation of the CCSLBM is extended to three dimensions. In three dimensions, the discrete Boltzmann-BGK equation can be written as

$$\frac{\partial f_k}{\partial t} + \boldsymbol{e}_k \cdot \nabla f_k = -\frac{1}{\tau}\left(f_k - f_k^{eq}\right), \quad k = 0,1,\ldots,18, \tag{37}$$

where the subscript k denotes the direction of the particle speed. In the D3Q19 discrete Boltzmann model (see Fig. 20), the microscopic velocities are given as [67]

$$\mathbf{e}_k = \begin{bmatrix} e_{kx} \\ e_{ky} \\ e_{kz} \end{bmatrix} = \begin{bmatrix} 0 & 1 & -1 & 0 & 0 & 0 & 0 & 1 & 1 & 1 & 1 & -1 & -1 & -1 & -1 & 0 & 0 & 0 & 0 \\ 0 & 0 & 0 & 1 & -1 & 0 & 0 & 1 & -1 & 0 & 0 & 1 & -1 & 0 & 0 & 1 & 1 & -1 & -1 \\ 0 & 0 & 0 & 0 & 0 & 1 & -1 & 0 & 0 & 1 & -1 & 0 & 0 & 1 & -1 & 1 & -1 & 1 & -1 \end{bmatrix}. \tag{38}$$

In this formulation, the equilibrium distribution function is defined as

$$f_k^{eq} = \alpha_k\left\{p + p_0\left[3(\boldsymbol{e}_k \cdot \boldsymbol{u}) + \tfrac{9}{2}(\boldsymbol{e}_k \cdot \boldsymbol{u})^2 - \tfrac{3}{2}(\boldsymbol{u} \cdot \boldsymbol{u})\right]\right\}, \tag{39}$$

where

$$\alpha_k = \begin{cases} \frac{2}{36}, & k = 1,2,\ldots,6 \\ \frac{1}{36}, & k = 7,8,\ldots,18 \\ \frac{12}{36}, & k = 0 \end{cases} \tag{40}$$

and the pressure p and the velocity vector $\boldsymbol{u}$ are obtained from the relations

$$p = \sum_{k=0}^{18} f_k, \quad p_0 \boldsymbol{u} = \sum_{k=0}^{18} \boldsymbol{e}_k f_k. \tag{41}$$

The 3D LB equation (37) can be written in the form

$$\frac{\partial f_k}{\partial t} = R_k, \tag{42}$$

where

$$R_k = -\left(e_{kx}\frac{\partial f_k}{\partial x} + e_{ky}\frac{\partial f_k}{\partial y} + e_{kz}\frac{\partial f_k}{\partial z}\right) - \frac{1}{\tau}\left(f_k - f_k^{eq}\right). \tag{43}$$

Again, the spatial derivatives in the 3D LB equation are discretized by the Chebyshev collocation spectral method to obtain high-accuracy solutions. Thus, the right-hand side of Eq. (42) can be written as

$$R_{k_{m,n,p}} = -\left(e_{kx}\sum_{i=0}^{N_x} D_{x_{m,i}} f_{k_{i,n,p}} + e_{ky}\sum_{i=0}^{N_y} D^T_{y_{i,n}} f_{k_{m,i,p}} + e_{kz}\sum_{i=0}^{N_z} D^T_{z_{i,p}} f_{k_{m,n,i}}\right) - \frac{1}{\tau}\left(f_{k_{m,n,p}} - f^{eq}_{k_{m,n,p}}\right), \tag{44}$$

where m, n, and p indicate the grid number in the x, y, and z directions, D_x indicates the derivative matrix in the x direction, and D_y^T and D_z^T are the transpose of the collocation derivative matrices in the y and z directions, respectively. In addition, N_x, N_y, and N_z are the polynomial degrees in each direction. Similar to the 2D simulations, the temporal term in Eq. (42) is discretized by the fourth-order Runge-Kutta scheme.

To apply the proposed method to an irregular geometry, one should use a mapping to transform the LB equation from the physical plane into the computational one. The calculation of the derivatives of the distribution function in the computational plane can be easily performed and the metrics and the Jacobian of the transformation should be calculated analytically if possible, or numerically with a high-order accuracy. Such a strategy has been used in literature for other LBM solvers (see, for example, [38,68]). The use of the spectral methods for solving the Navier-Stokes equations in the generalized curvilinear coordinate has also been applied in the literature (see, for example, [69,70]). Thus, the implementation of the CCSLBM in the generalized curvilinear coordinate seems to be straightforward.

VIII. NUMERICAL RESULTS FOR A 3D PROBLEM

A. Steady flow in a three-dimensional regularized cavity

In the previous test cases, the CCSLBM has been implemented to solve different 2D problems and now it can be used for more interesting 3D flows. Herein, the 3D accurate developed code is used to compute the flow in a regularized cubic cavity. The no-slip boundary conditions are used for all the velocity components on all the walls except for the upper wall. Three lid velocity profiles are considered in the upper wall boundary as follows:

$$u_1 = u_0[16x(1-x)y(1-y)], \quad v = w = 0, \tag{45}$$

$$u_2 = u_0[16x(1-x)y(1-y)]^2, \quad v = w = 0, \tag{46}$$

$$u_3 = u_0[1-(2x-1)^{18}]^2[1-(2y-1)^{18}]^2, \quad v = w = 0. \tag{47}$$

The calculations are performed for the computational $25 \times 25 \times 25$ grid and for different flow conditions. The three-dimensional cavity geometry and three velocity distributions on the upper wall are shown in Fig. 21. For u_1, the mean value of this distribution over the driving surface is $u_m = 0.85u_0$, and the area over which the velocity is above the mean value is 75% that of the lid [71]. Figure 22 shows the graphs of u/u_0–z and w/u_0–x at the midlines of the cavity ($x = 0.5$, $y = 0.5$ and $y = 0.5$, $z = 0.5$, respectively) and for the three velocity distributions u_1, u_2, and u_3 for the upper wall for $\mathrm{Re} = 100$, 400, and 1000 in which the Reynolds number is defined as $\mathrm{Re} = u_0 L/\upsilon$. As shown in this figure, the results obtained by implementing the CCSLBM in three dimensions for the

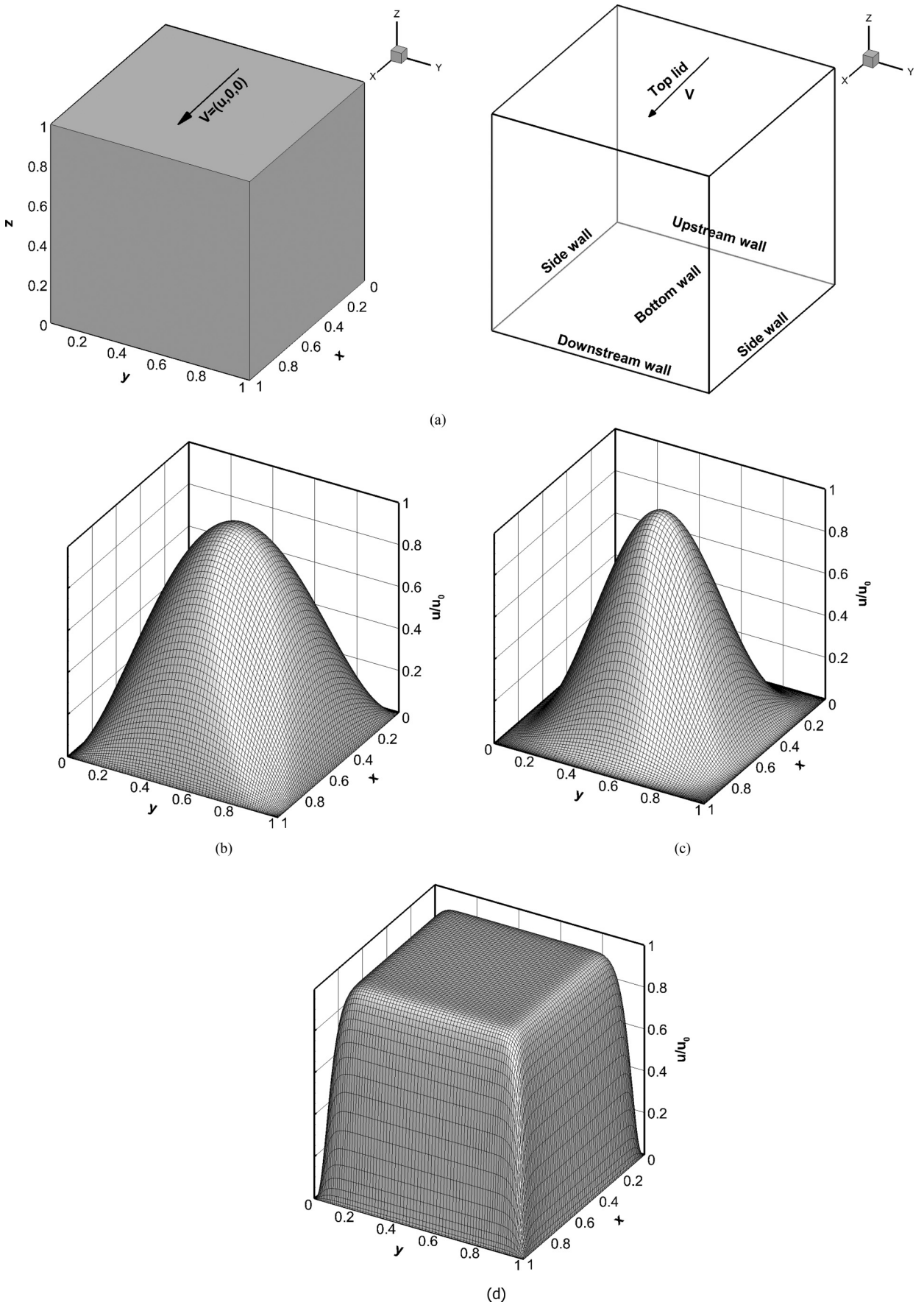

FIG. 21. The (a) 3D regularized cavity problem and (b)–(d) different velocity distributions (b) u_1, (c) u_2, and (d) u_3 for the upper wall.

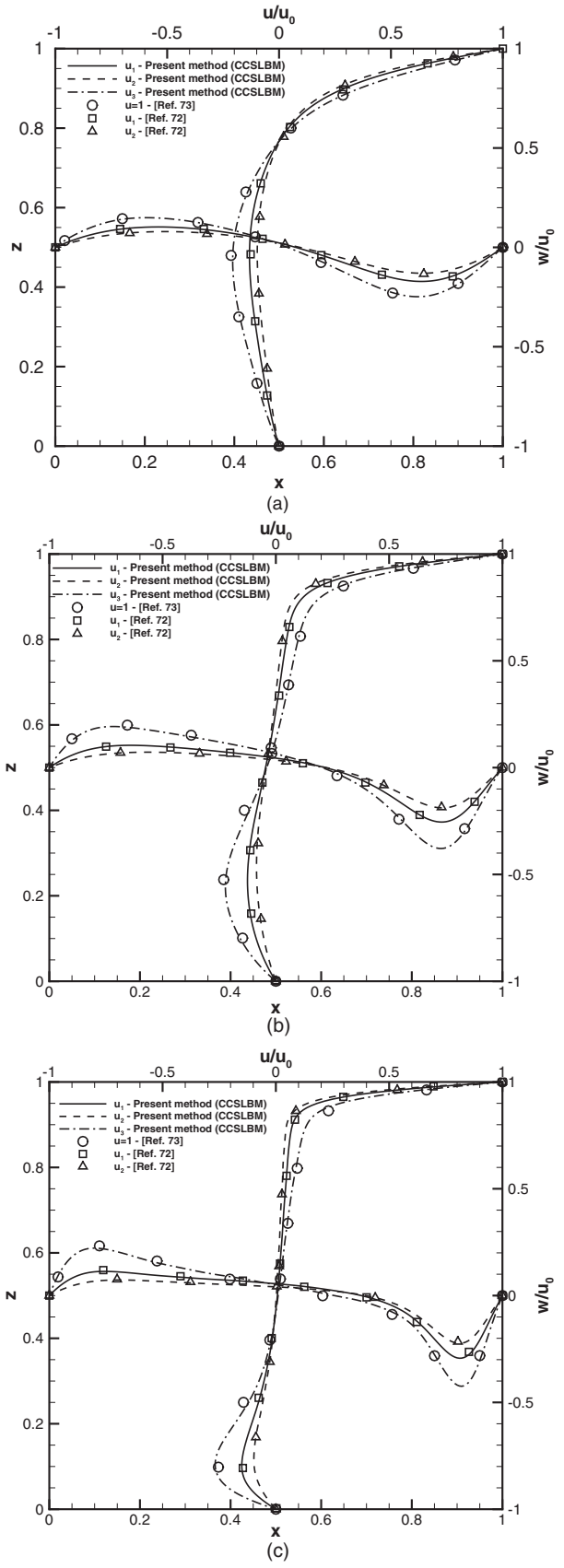

FIG. 22. Comparison of velocity profiles at the midplanes of the 3D regularized cavity for (a) Re = 100, (b) Re = 400, and (c) Re = 1000.

velocity distributions u_1 and u_2 are comparable to those of the finite-element solution of the Navier-Stokes equations by Notsu [72]. Note that in [72] the same velocity distributions u_1 and u_2 are used for the upper lid wall. For the u_3 velocity distribution, good agreement between the present solution, applying the CCSLBM, and that of the higher-order compact Navier-Stokes flow solver [73] is observed. Note that in [73] a uniform velocity distribution ($u = 1$) for the upper lid wall was used and the present study shows that using the velocity distribution u_3 provides similar results and thus similar flow structures. As shown in Fig. 22, choosing a nearly uniform velocity distribution with higher-velocity magnitudes over the upper cavity wall results in increasing the gradient of the velocity normal to the walls and thus causes higher viscous shear forces there. Increasing the value of the Reynolds number has a similar effect. The computed flow field shown by the streamlines in the y–z ($x = 0.5$), x–z ($y = 0.5$), and x–y ($z = 0.5$) planes for Re = 100, 400, and 1000 using the velocity distribution u_3 is shown in Fig. 23. As observed in this figure, due to the effect of the sidewalls, the flow patterns in the y–z plane show a pair of counterrotating vortices. Also a pair of small counterrotating vortices can be seen near the upper corners at Re = 1000. The results indicate that with increasing Re, the centers of the centered vortices are moved considerably toward the bottom wall and the vortices near the corners grow. This primary recirculating region and also the secondary vortices near the corners in the x–z plane are seen for each case. It is observed that with increasing Re, the center of the primary vortex is moved toward the center of the cavity, as also seen in the 2D cavity flow. In addition, in the x–y plane with increasing Re two vortices are created and move toward the downstream wall due to the increasing momentum and inertia. This indicates that the CCSLBM can be used as a capable and accurate flow solver for simulating 3D flow problems.

IX. CONCLUSION

A Chebyshev collocation spectral lattice Boltzmann method is proposed and applied to accurately compute steady and unsteady low speed flows. Herein, the discrete Boltzmann equation with the BGK approximation based on the pressure distribution function is considered and the spatial derivatives in this formulation are discretized by the Chebyshev collocation spectral method and the temporal term was discretized by the fourth-order Runge-Kutta scheme to provide a highly accurate LBM-based flow solver. The calculations are performed for different 2D and 3D problems to examine the accuracy and robustness of the Chebyshev collocation spectral LBM. Some conclusions and remarks regarding the present work are as follows.

(i) The study shows that the calculated results obtained by applying the Chebyshev collocation spectral LBM exhibit excellent agreement with the analytical and numerical results. The results obtained by the Chebyshev collocation spectral LBM are thoroughly compared and verified with those of spectral Navier-Stokes flow solvers. Comparisons indicate that both the solution methodologies give nearly the same results for the same grid size. Indications are that the present solution methodology, that is, the Chebyshev collocation

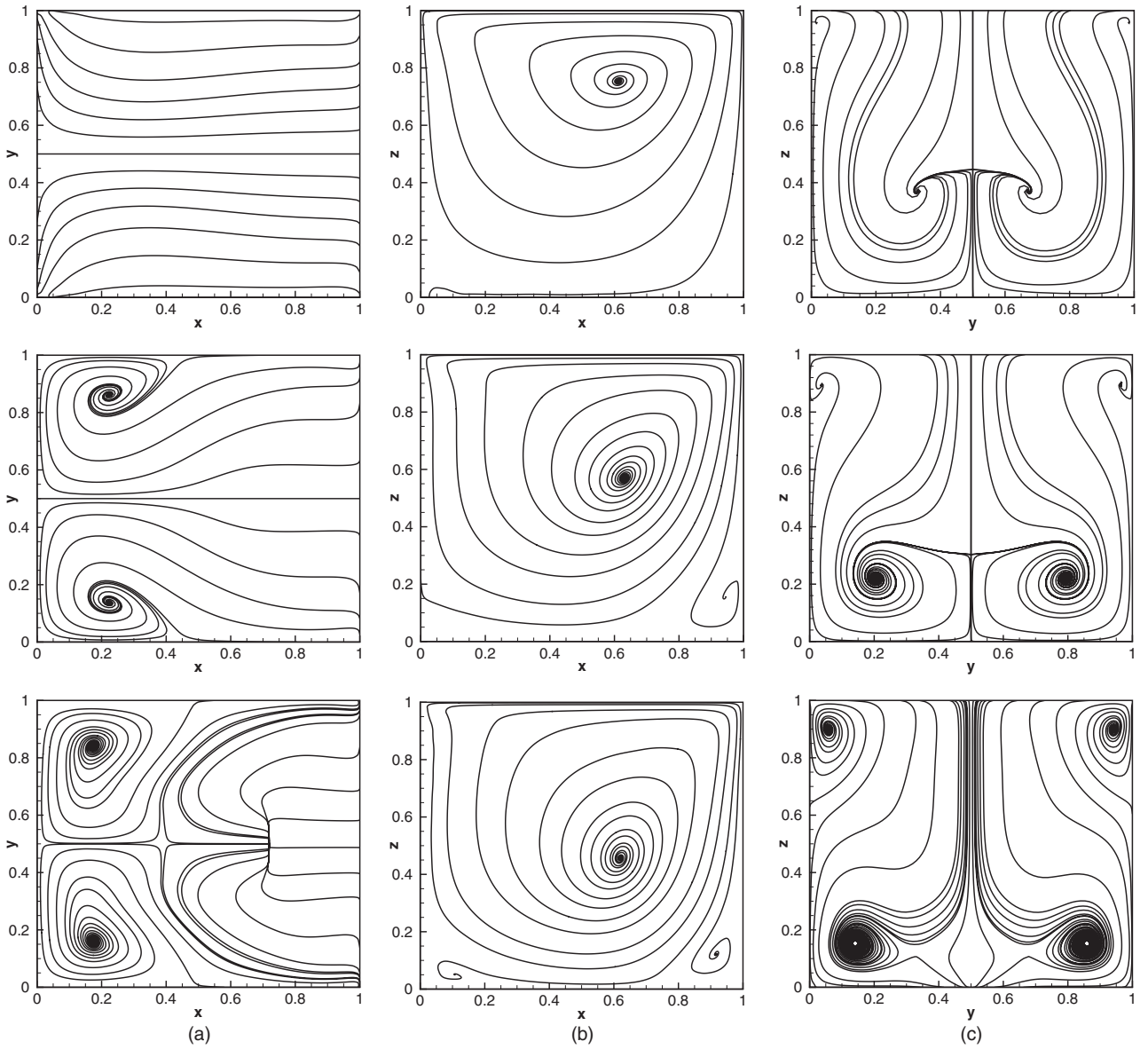

FIG. 23. Computed flow field for the 3D regularized cavity shown by streamlines for Re = 100 (top row), Re = 400 (middle row), and Re = 1000 (bottom row) and the x–y midplane (left column), x–z midplane (middle column), and (c) y–z midplane (right column).

spectral LBM, can be considered as a suitable alternative to spectral Navier-Stokes flow solvers, due to the simplicity of its formulation to implement.

(ii) A proper implementation of the boundary conditions is essential to have both numerical stability and accuracy for the spectral methods. In this study, physical boundary conditions based on the spectral solution of the governing equations implemented on the boundaries are used to address these issues. The results indicate that such a boundary treatment gives stable solutions for the Chebyshev collocation spectral LBM and provides accurate results in the whole solution domain.

(iii) An iterative procedure is applied to generate consistent initial conditions for the distribution function and the pressure field for the Chebyshev collocation spectral LBM. The present study shows that such a procedure can remove some possible errors that may arise in unsteady flow simulations and can provide accurate and reliable unsteady solutions comparable to the analytical results.

(iv) The simulations performed by applying the Chebyshev collocation spectral LBM verify the exponential convergence of the solution when the error is evaluated for each grid compared with the solution of the most refined one. They also indicate that the value of the characteristic velocity should be selected as small as possible to reduce the compressibility effects leading to more accurate solutions. By choosing small values of the characteristic velocity, the spectral convergence of the solution is also verified by calculating the error for each grid compared with the analytical solution.

(v) The computational efficiency of the proposed solution methodology based on the Chebyshev collocation spectral LBM is examined by comparison with those of the standard streaming-collision (classical) LBM and two finite-difference LBM solvers, namely, the fourth-order compact

finite-difference LBM and the developed second-order central finite-difference LBM. It is demonstrated that the CCSLBM reduces the CPU time and memory usage compared to these LBM solvers when a high-accuracy solution is required and the performance of the CCSLBM is highlighted in such conditions.

(vi) Unlike other high-order accurate numerical methods used to solve the LB equation, the Chebyshev collocation spectral LBM applied here does not need any numerical dissipation or filter for the solution to be stable and that leads to highly accurate solutions. The decay of the error at exponential rather than polynomial rates and free of both dissipation and dispersive errors are the main advantages of using the Chebyshev collocation spectral LBM compared to other LBM methods. Note that high-accuracy solutions obtained by applying the Chebyshev collocation spectral LBM can be used as benchmark solutions for verifying the results of other LBM-based flow solvers.

(vii) The extension of the Chebyshev collocation spectral LBM for simulating 3D flow problems is also performed and the capability and accuracy of the solution methodology developed are demonstrated by computing a 3D regularized cavity flow for different flow conditions. The present computations indicate that the Chebyshev collocation spectral LBM implemented is robust, efficient, and accurate for solving 2D and 3D, steady and unsteady low-speed flows. Such a stable and highly accurate flow solver can be a reliable tool to precisely study the physics of more complicated flows such as transitional and turbulent flows.

ACKNOWLEDGMENT

The authors would like to thank Sharif University of Technology for the support of this research.

[1] G. R. McNamara and G. Zanetti, Phys. Rev. Lett. **61**, 2332 (1988).
[2] F. J. Higuera and S. Succi, Europhys. Lett. **8**, 517 (1989).
[3] F. J. Higuera, S. Succi, and R. Benzi, Europhys. Lett. **9**, 345 (1989).
[4] R. Benzi, S. Succi, and M. Vergassola, Phys. Rep. **222**, 145 (1992).
[5] D. A. Wolf-Gladrow, *Lattice Gas Cellular Automata and Lattice Boltzmann Models* (Springer, Berlin, 2000).
[6] M. Watari, Phys. Rev. E **79**, 066706 (2009).
[7] Y. H. Qian, D. d'Humières, and P. Lallemand, Europhys. Lett. **17**, 479 (1992).
[8] Y. Shi, T. S. Zhao, and Z. L. Guo, Phys. Rev. E **73**, 026704 (2006).
[9] S. Marconi, B. Chopard, and J. Latt, Mod. Phys. C **14**, 1015 (2003).
[10] H.-p. Fang, R.-z. Wan, and Z.-f. Lin, Phys. Rev. E **66**, 036314 (2002).
[11] Z. L. Guo, B. Shi, and N. Wang, Comput. Phys. **165**, 288 (2000).
[12] X. He and L. Luo, Stat. Phys. **88**, 927 (1997).
[13] Q. Zou, S. Hou, S. Chen, and G. D. Doolen, Stat. Phys. **81**, 35 (1995).
[14] Y. Chen and H. Ohashi, Mod. Phys. C **08**, 793 (1997).
[15] O. Filippova and D. Hanel, Comput. Phys. **147**, 219 (1998).
[16] R. Du, B. Shi, and X. Chen, Phys. Lett. A **359**, 564 (2006).
[17] M. E. McCracken and J. Abaham, Phys. Rev. E **71**, 036701 (2005).
[18] M. Geier, A. Greiner, and J. G. Korvink, Eur. Phys. J. Spec. Top. **171**, 55 (2009).
[19] M. Geier, A. Greiner, and J. G. Korvink, Phys. Rev. E **73**, 066705 (2006).
[20] J. Wu and C. Shu, Comput. Phys. **230**, 2246 (2011).
[21] D. Yu, R. Mei, and W. Shyy, Numer. Methods Fluids **39**, 99 (2002).
[22] A. Duster, L. Demkowicz, and E. Rank, Numer. Methods Eng. **67**, 1094 (2006).
[23] X. Shi, J. Lin, and Z. Yu, Numer. Methods Fluids **42**, 1249 (2003).
[24] M. Min and T. Lee, Comput. Phys. **230**, 245 (2011).
[25] T. Lee and C.-L. Lin, Comput. Phys. **185**, 445 (2003).
[26] T. Lee and C.-L. Lin, Comput. Phys. **171**, 336 (2001).
[27] Y. Li, E. J. LeBoeuf, and P. K. Basu, Phys. Rev. E **72**, 046711 (2005).
[28] M. Stiebler, J. Tolke, and M. Krafczyk, Comput. Fluids **35**, 814 (2006).
[29] V. Patil and K. N. Lakshmisha, Comput. Phys. **228**, 5262 (2009).
[30] H. Xi, G. Peng, and S.-H. Chou, Phys. Rev. E **59**, 6202 (1999).
[31] F. Dubois and P. Lallemand, Prog. Comput. Fluid Dyn. **8**, 11 (2008).
[32] H. Chen, Phys. Rev. E **58**, 3955 (1998).
[33] S. Ubertini, G. Bella, and S. Succi, Phys. Rev. E **68**, 016701 (2003).
[34] V. Sofonea and R. F. Sekerka, Comput. Phys. **184**, 422 (2003).
[35] M. B. Reider and J. D. Sterling, Comput. Fluids **24**, 459 (1995).
[36] J. Tolke, M. Krafczyk, M. Schulz, and E. Rank, Mod. Phys. C **09**, 1143 (1998).
[37] A. Xu, Phys. Rev. E **71**, 066706 (2005).
[38] Z. Guo and T. S. Zhao, Phys. Rev. E **67**, 066709 (2003).
[39] L. Wu, M. Tsutahara, and S. Tajiri, Fluids Sci. Technol. **2**, 35 (2007).
[40] M. Watari and M. Tsutahara, Phys. Rev. E **67**, 036306 (2003).
[41] S. C. Fu, R. M. C. So, and W. W. F. Leung, Comput. Phys. **229**, 6084 (2010).
[42] Y. Shi, T. S. Zhao, and Z. L. Guo, Comput. Fluids **35**, 1 (2006).
[43] R. Mei and W. Shyy, Comput. Phys. **143**, 426 (1998).
[44] K. Hejranfar and E. Ezzatneshan, Int. J. Numer. Methods Fluids **75**, 713 (2014).
[45] E. Leriche, J. Sci. Comput. **27**, 335 (2006).
[46] J. Shen, J. Comput. Phys. **95**, 228 (1991).
[47] M. Rudmanand and H. M. Blackburn, Appl. Math. Model. **30**, 1229 (2006).
[48] R. Mei, L. Luo, and W. Shyy, J. Comput. Phys. **155**, 307 (1999).
[49] B. Fornberg, *A Practical Guide to Pseudospectral Methods* (Cambridge University Press, Cambridge, 1996).

[50] S. R. Fulton and W. H. Schuber, Mon. Weather Rev. **115**, 1940 (1987).
[51] M. T. Darvishi, Int. Math. Forum **2**, 263 (2007).
[52] R. Baltensperger, Appl. Numer. Math. **33**, 143 (2000).
[53] R. Baltensperger and J. P. Berrut, Comput. Math. Appl. **37**, 41 (1999).
[54] C. Canuto, M. Y. Hussaini, A. Quarteroni, and T. A. Zang, *Spectral Methods Evolution to Complex Geometries and Applications to Fluid Dynamics* (Springer, New York, 2007).
[55] B. Costa, Cubo-Revista de Matemática **6**, 1 (2004).
[56] K. S. Breuer and E. M. Everson, J. Comput. Phys. **99**, 56 (1992).
[57] W. S. Don and A. Solomonoff, SIAM J. Sci. Comput. **16**, 1253 (1995).
[58] C. Schneider and W. Werner, Math. Comput. **47**, 285 (1986).
[59] R. Mei, L. Luo, P. Lallemand, and D. d'Humieres, Comput. Fluids **35**, 855 (2006).
[60] J. Martinez and P. Esperanca, J. Braz. Soc. Mech. Sci. Eng. **29**, 317 (2007).
[61] O. Botella, Comput. Fluids **26**, 107 (1997).
[62] U. Ehrenstein and R. Peyret, Int. J. Numer. Methods Fluids **9**, 427 (1989).
[63] G. I. Taylor, Philos. Mag. **46**, 671 (1923).
[64] M. L. Minion and D. L. Brown, Comput. Phys. **138**, 734 (1997).
[65] P. J. Dellar, Phys. Rev. E **64**, 031203 (2001).
[66] D. Ricot, S. Marié, P. Sagaut, and C. Bailly, Comput. Phys. **228**, 4478 (2009).
[67] M. Hecht and J. Harting, J. Stat. Mech.: Theory Exp. (2010) P01018.
[68] K. Hejranfar and E. Ezzatneshan, J. Comput. Phys. **267**, 28 (2014).
[69] R. Mittal and S. Balachandar, J. Comput. Phys. **124**, 351 (1996).
[70] M. Kotovshchikova, Appl. Math. Sci. **5**, 1649 (2011).
[71] L. Leriche and S. Gavrilakis, Phys. Fluids **12**, 1363 (2000).
[72] H. Notsu, Jpn. Soc. Comput. Eng. Sci. **2008**, 1 (2008).
[73] K. Hejranfar and A. Khajeh-Saeed, Numer. Methods Fluids **66**, 939 (2011).